



## Harbor geoarchaeology and urban change in the ancient Knidia (SW Türkiye)

H. Delile<sup>a,\*</sup>, J. Leidwanger<sup>b</sup>, J.-P. Goiran<sup>a</sup>, J. Blichert-Toft<sup>c</sup>, F. Stock<sup>d</sup>, G. Brocard<sup>a</sup>, L. Radloff<sup>e</sup>, E.S. Greene<sup>f</sup>, N. Tuna<sup>g</sup>

<sup>a</sup> CNRS, Archéorient, UMR 5133, Maison de l'Orient et de la Méditerranée, University of Lyon 2, Lyon, France

<sup>b</sup> Department of Classics, Stanford University, Stanford, CA, United States

<sup>c</sup> Ecole Normale Supérieure de Lyon and CNRS, 69007, Lyon, France

<sup>d</sup> Baden-Württemberg State Institute for the Environment, Hertzstraße 173, 76187, Karlsruhe, Germany

<sup>e</sup> Department of Historical Studies, University of Toronto Mississauga, Mississauga, ON, Canada

<sup>f</sup> Department of Classics and Archaeology, Brock University, St Catharines, ON, Canada

<sup>g</sup> Institute of Social Sciences, Program of Settlement Archaeology, Middle East Technical University, Ankara, 06800, Türkiye

### ARTICLE INFO

Handling Editor: Dr Mira Matthews

**Keywords:**

Harbor geoarchaeology

Pb isotopes

Palaeo-pollution

FTIR-ATR

Ore provenance

Burgaz

Knidos

Eastern Mediterranean

Environmental history

### ABSTRACT

The relationship between the two major centers on the Datça Peninsula at Burgaz and Knidos—and the potential shift in population and centrality from one to the other around the 4<sup>th</sup> c. BCE—casts a long shadow over the history of the region known in antiquity as the Knidia. What prompted the shift remains unclear in the historical records, but it must have represented a strategic collective decision and major civic investment. Underwater archaeological excavations revealed a 3-m stratigraphic section in the earliest harbor basin of Burgaz, offering a window into the environmental context in which Burgaz flourished and gave way to Knidos at the tip of the peninsula. This study investigates whether socio-environmental systems contributed to this shift, focusing on changes in natural conditions and lead contamination. Anthropogenic lead excesses reveal a first isotopic fingerprint of exogenous lead, linked to central Greece and the Cyclades before the 2<sup>nd</sup> c. BCE. Knidos, strategically located at the intersection of Aegean and eastern Mediterranean and Levantine maritime routes, served as a pivotal hub in these networks. During the Roman centuries that followed, though, the source of lead reoriented towards the northern Aegean, offering a new window into potential changes in Knidos's function as an intermediary hub in the emerging imperial trade system. Following the foundation of the city, the basin was excavated around 2600 cal BP, after which it experienced a twofold increase in seafloor aggradation due to the creation of new accommodation space and increased terrigenous inputs driven by Burgaz's pivotal role in the region's agricultural economy. Despite the development of other facilities at Burgaz, Knidos, and elsewhere along the coast, the maintenance of this original harbor continued, with a second dredging phase in Late Antiquity. This may reflect a deliberate effort to sustain a multi-scale harbor system across the peninsula.

### 1. Introduction

The site of Burgaz, on the Datça Peninsula in southwest Türkiye (Fig. 1), provides a rich context to explore socioeconomic relations, community development, and interactions between environmental and social changes within a well-preserved maritime landscape. The city's four partially infilled harbor basins attest to nearly three millennia of maritime culture along a seismically active 1 km stretch of coast. Indeed, from at least the Archaic period and into the Hellenistic and Roman periods, the peninsula's strategic position along key maritime routes

connecting the Aegean and western Asia Minor to the eastern Mediterranean and Near East allowed the region to grow as a key trading hub (Greene et al., 2019). One of the most significant events in its history was the rapid rise of the city of Knidos at Tekir, 30 km to the west on the western tip of the peninsula (Fig. 1B), especially from around the mid-4<sup>th</sup> c. BCE (Bean and Cook, 1952; Bresson, 1999). The growth and increasing prominence of Knidos coincided with a fundamental transformation at Burgaz, which saw the development of new industry in place of the civic center as well as expanded agricultural lands in its hinterland (Tuna et al., 2009). Despite this reorganization of activities

\* Corresponding author.

E-mail address: [hugo.delile@cnrs.fr](mailto:hugo.delile@cnrs.fr) (H. Delile).

across the peninsula, some harbors of Burgaz remained active until the later Roman era (Late Antiquity), seemingly for the transport of processed agricultural goods packaged in locally produced amphoras (Leidwanger et al., 2015; Greene et al., 2019).

Such reorganization of activities involves a substantial economic and civic investment, so the decision may have been considered for many years and reflected the culmination of collective processes that are often not recorded in historical documents or immediately observable in the archaeological record. We evaluate the possibility that natural phenomena, reflecting either sudden or gradual change, ultimately influenced this decision. For instance, we consider the potential contribution of natural disasters, such as earthquakes (Guidoboni et al., 1994; Altunel et al., 2003; Özsayın et al., 2021), tsunamis (Bruins et al., 2008; Vött

et al., 2018; Delile and Salomon, 2020; Lespez et al., 2021; Gogou et al., 2022) and storms (Marriner et al., 2017; Vandarakis et al., 2021), which are common in the study area. We also consider the possibility of progressive or sudden submersion of the harbor infrastructure due to land subsidence. This process has already been documented at certain points along the coast at Burgaz, where Özsayın et al. (2021) calculated a tectonic subsidence of 0.95–1.20 m for harbor basin 1 (L1, for “Liman 1” in Turkish) (i.e., a subsidence rate of 0.36–0.46 mm yr<sup>-1</sup>) and 2.75–3.00 m for harbor basins 2 (L2) and 3 (L3) (i.e., a subsidence rate of 1.05–1.15 mm yr<sup>-1</sup>). Combined with glacio-hydro-isostatic changes (e.g., Lambeck and Bard, 2000; Lambeck and Purcell, 2005; Lambeck et al., 2014), tidal range variations (e.g., Goiran et al., 2011a; Hall et al., 2013), and coastal progradation (e.g., Törnqvist et al., 2008; Marriner

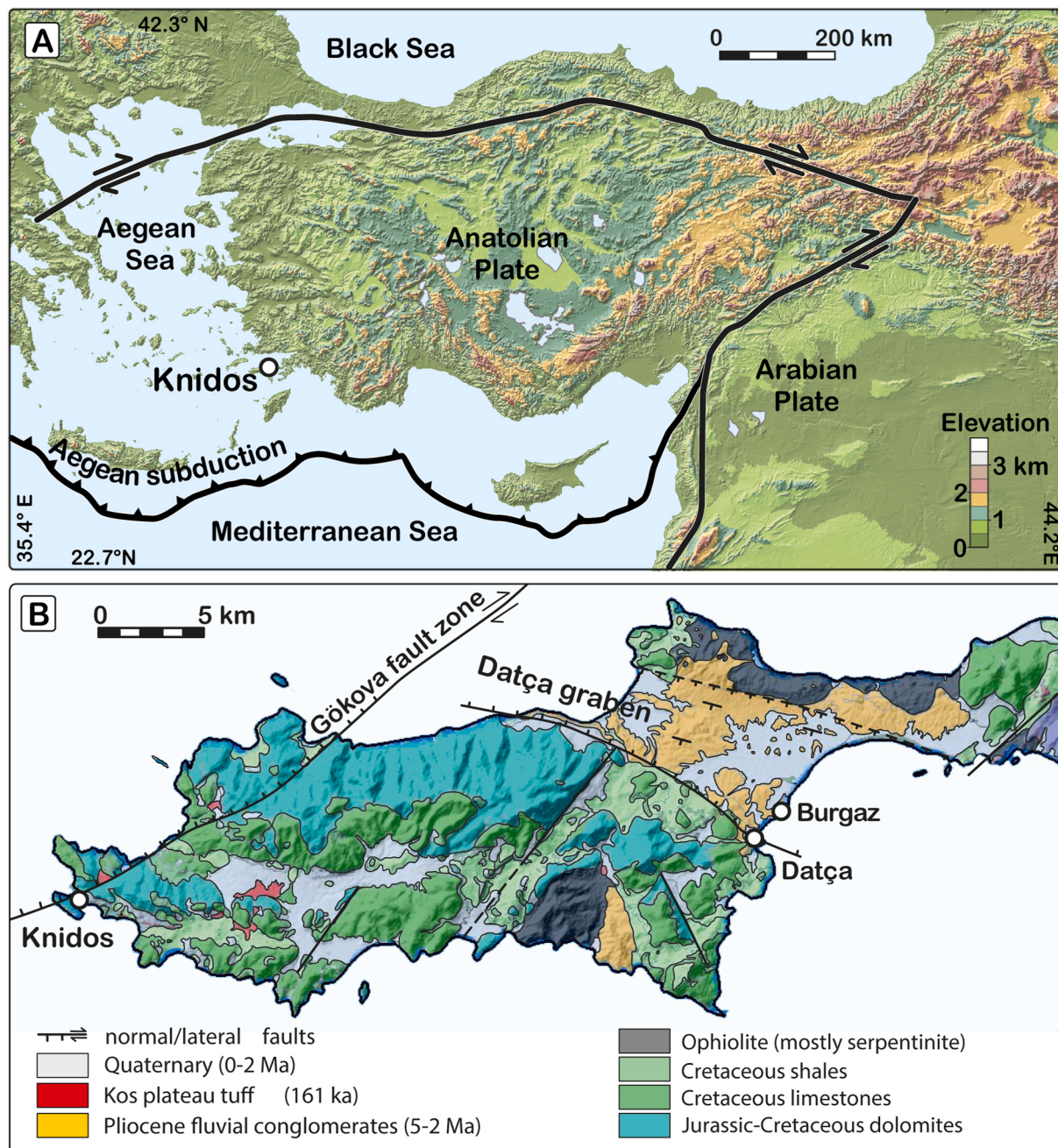


**Fig. 1.** (A) Topographic map of Anatolia and the Aegean Sea showing the location of Knidos and Burgaz, and of the Anatolian microplate tectonic boundaries. (B) Geological map of the Datça Peninsula (1:100,000 geological maps of the General Directorate of Mineral Research and Exploration of Türkiye) showing unambiguous Plio-Quaternary tectonic faults (offshore fault from İşcan et al., 2013).

et al., 2012), this morpho-structural process (e.g., Flemming et al., 1971; Pirazzoli et al., 1994; Kayan, 1988; Nelson et al., 1996) defines the Holocene relative sea-level rise (e.g., Goiran et al., 2011a; Vacchi et al., 2016). Subsequent to decreasing rates of relative sea-level rise around 6700 years ago (Lambeck et al., 2014), coastal landscapes were fixed. Maritime communities were thus more able to build port infrastructure to support communication networks since the Bronze Age, through which they developed and prospered.

At regional and local scales, the variability in relative influence of these natural processes has led to the formation of diverse coastal geomorphologies. These are reflected in how environmental factors shape the geoarchaeological typologies of ancient ports, where each category—fluvial, lagoonal, and artificial harbors, as well as rocky bays and promontories—experienced different impacts, such as marine erosion, flood inundation, siltation, neotectonic activity, storms, and tsunamis, each with varying magnitudes (Marriner and Morhange, 2007; Giaime et al., 2019). One of the most significant and widespread hazards affecting the resilience and sustainability of ancient ports is siltation, which is induced by shoreline progradation processes such as direct fluvial sediment inputs, longshore drift, human-induced soil erosion, and the addition of maritime facilities designed for port accessibility. To address this challenge, various adaptation measures have been implemented. Notable examples include the mole design of the harbor of Claudius at Portus near Rome (e.g., Keay et al., 2005; Keay, 2012; Goiran et al., 2010), the dredging operations at Neapolis (e.g., Marriner and Morhange, 2007; Carsana et al., 2009; Delile et al., 2016a), the transformation at Portus from just the open Claudian basin via the addition of a closed inner basin under Trajan (e.g., Keay et al., 2005; Keay, 2012; Goiran et al., 2011b) and their interconnection via Portus's network of canals (e.g., Salomon et al., 2012, 2014). The changing locations of harbor basins in Ephesus are also noteworthy (e.g., Stock et al., 2013, 2014). The most extreme adaptative response that highlights the critical need to keep ports accessible is the large-scale relocation of a city. Such incidents were rare but occasionally prompted by environmental factors, alongside other related considerations, as illustrated by the abandonment of Pi-Ramesses in the early 12<sup>th</sup> c. BCE (Hoffmeier and Rendsburg, 2022) in favor of Tanis (Graham, 1997) due to the silting of the Pelusiac branch of the Nile River (Bietak, 1981). Social factors also played a role in such shifts and these occasional relocations of ancient cities. For example, the destruction of Sybaris by the neighboring city of Kroton at the end of the 5<sup>th</sup> c. BCE led to the founding of Thurii, which was partially built on the remains of the older city (Evans, 2014). This was also the case in Aegean Thrace, where Mayoral et al. (2024) argued that the city of Abdera was relocated in the 4<sup>th</sup> c. BCE due to military upheavals rather than the silting of its harbor basin. Environmental and other factors must often have worked together to influence a decision, as is certainly evident in the choice to shift major port operations and investment from Puteoli and Ostia to Portus in the mid-1<sup>st</sup> c. AD in an effort to address both the silting up of the Ostia harbor and imperial Rome's need to expand its capacity for commercial maritime traffic closer to Rome (Keay et al., 2005; Keay, 2012; Goiran et al., 2014).

Against this backdrop, we conduct an environmental assessment to determine how environmental and/or related social factors may have influenced the motivation behind the shifting of activities along the Datça Peninsula around the 4<sup>th</sup> c. BCE. In this respect, we rely on sediment deposits of the earliest and longest-lived harbor basin (L1) at Burgaz (Fig. 1) using reliable chronostratigraphy models, grain size distribution analysis, and geochemical analyses. Trace metal element (TME) concentrations and lead (Pb) isotope compositions are particularly useful for tracking long-term urban activities and gauging some local maritime connections associated with Pb ores (Delile and Keenan-Jones, 2024).

## 2. Geographical and historical setting

### 2.1. Study area

The Datça Peninsula stretches over 60 km and is highly mountainous, with elevations reaching up to 1120 m above sea level (a.s.l.). Between Burgaz and Knidos, the mountains are composed of Cretaceous dolomites, limestones, and shales, with some areas overlain by serpentinite (Fig. 1B). A saddle halfway through the peninsula is filled with Pliocene sediments (Kayan, 1988) and forms the Knidia's fertile hinterland. The older city at Burgaz was situated in the bay east of modern Datça, to the southwest of the Uzunazmak River delta. At the end of the peninsula at Tekir, Knidos sits on a hill summit composed of Pliocene conglomerates, which is cut by a sea cliff 200 m long and 15 m high. Burgaz developed four harbor basins (L1-L4) in small embayments—now partially infilled—to the southwest and northeast of the acropolis (Fig. 2). The acropolis hill is intersected by a vertical fault that disrupts the shallow-dipping Pliocene fluvial facies and contains deposits suggesting a former major groundwater pathway.

The Datça Peninsula sits in one of the most seismically active regions of the Mediterranean, near where the Mediterranean seafloor plunges beneath the overriding Anatolian-Aegean tectonic microplate (Fig. 1A) in a trench located south of Crete and Rhodes, at a rate of 2.5 cm/y (Reilinger et al., 2010). There, the subducted slab plunges to the north, as evidenced by the volcanic arc (Kos and Nisyros islands) and the extensional grabens bound by normal faults. The overriding Anatolian-Aegean plate, on which the settlements are located, is currently undergoing crustal extension, resulting in the linear submersion of vast land areas between continental Greece and Anatolia.

The harbors along the peninsula are situated in a region that has experienced ongoing ground subsidence over the past two millennia and are now below sea level. Submersion values range from 2.4 m below sea level (b.s.l.) to 4.5 m b.s.l. along this stretch of coast (Anzidei et al., 2011), with the deepest parts of L1 and L2/L3 (Fig. 2) reaching 2.2 m b.s.l. and 4.0 m b.s.l., respectively (Özsayın et al., 2021). Based on a sea level 2600 years ago that was 1.0–1.25 m b.s.l., Özsayın et al. (2021) estimate a tectonic subsidence of 0.95–1.20 m for the L1 basin. However, depending on the sea level chosen for that time, the ranges of subsidence values can vary significantly. The timing of the subsidence is unknown but predates the Little Ice Age (AD 1450–1850) (Kızıldağ et al., 2012). Subsidence thus has a clear tectonic component, but the specific sources are currently unknown. It could be the result of the close repetition of smaller earthquakes on the faults surrounding the peninsula during an earthquake swarm, as suggested for the Gulf of Corinth (Boulton and Stewart, 2015). Alternatively, the regional pattern of subsidence may have not been episodic, but rather continuous, due to slow, aseismic downward bending of the Anatolian plate.

### 2.2. Historical and archaeological background

The settlement at Burgaz was already known to the travelers of the 19<sup>th</sup> and early 20<sup>th</sup> centuries (Newton, 1865; Spratt, 1886; cf. Pliny, NH 5.29). Bean and Cook (1952) visited in the mid-20<sup>th</sup> c., revising the early topographical interpretations and putting forward the theory of the dual “Old” and “New” Knidos. They suggested that the original Knidian center was located at Burgaz and the later Hellenistic settlement at Tekir, postulating a transfer around the beginning of the Hellenistic period, although they rejected the notion that the earlier site was completely abandoned. Such a shift, Bean and Cook (1952) note, was common among cities of the Dorian pentapolis, a federation of regional Dorian Greek settlements that included Knidos, Kos, Lindus, Ialyssus, and Kamirus (Hdt. 1.144). Communities might leave their old locations to gain more advantageous positions in response to shifting maritime routes: for example, this may have motivated the collaborative foundation of the city of Rhodes toward the end of the 5<sup>th</sup> c., situating them well to capitalize on the increasingly busy sea lanes that connected the

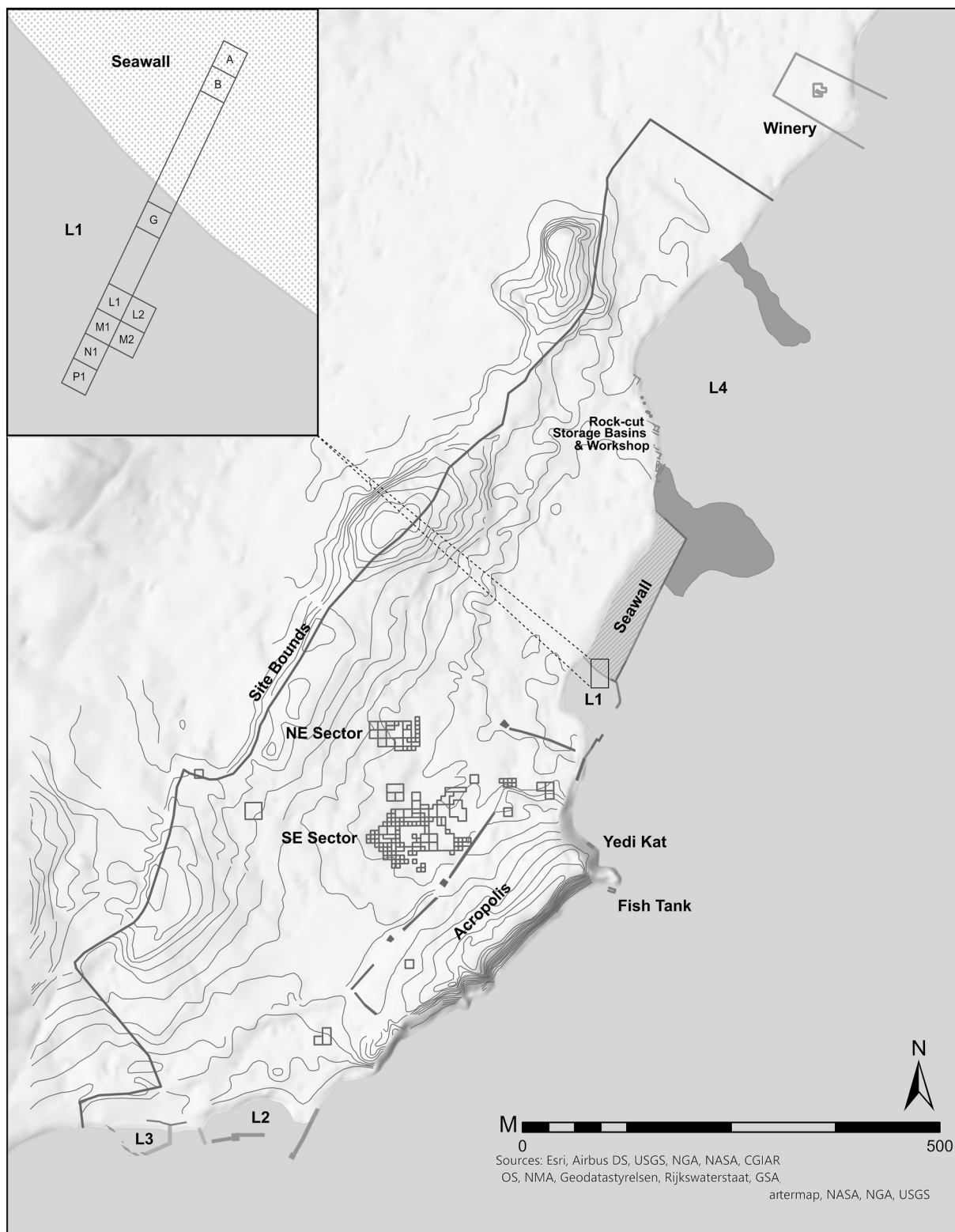


**Fig. 2.** (A) Plan of Burgaz showing key features, harbor basins (L1–L4), and a zoomed-in view of Trench 5 (T5), in which the stratigraphic section was excavated in Unit P1. The upper right quadrant provides a detailed view of the excavation area within the earliest harbor basin (L1). Dark grey areas indicate submerged port structures, as identified from aerial imagery.

Aegean to the eastern Mediterranean and beyond (Tuna et al., 2009; Greene et al., 2019). Much scholarly contention, though, surrounds Bean and Cook's relocation theory, and its topography remains unresolved, partly due to accounts in the primary sources mentioning Knidos that conflict with the various locations along the peninsula (Tuna, 1983,

1988, 1995, 1997, 1998, 2004; Tuna et al., 2009; Demand, 1989, 1990; Blümel, 1992; Özgan, 1995; Berges, 1994; Bresson, 1999). Historical accounts testify to Knidos's strategic importance within local, regional, and interregional networks from at least the 6<sup>th</sup> c. BCE, due to its location (Hdt. 1.174; Paus. 2.1.5; Diod. 14.83; Str. 14.2.15; cf. Ruzicka,

2012) and use as a sea base (Thuc. 8.35, 8.42–4, 8.109) for refuge (Xen. Hell. 4.8.19; Diod. 14.99) and for the suppression of nearby poleis (Xen. Hell. 4.8.20–24; cf. Tuna et al., 2009). Whatever the reality behind any true “relocation” of the city, it is clear that Burgaz was eclipsed by Knidos as the major center on the peninsula, and both sites served discrete and complementary roles within the economy and society of the Datça Peninsula during that period and after. The key question is, then, what role different pressures and opportunities may have had on this trajectory of change and the dynamics it fostered.

The settlement at Burgaz was occupied since at least the early 8<sup>th</sup> c. BCE and rose as a maritime center over the course of the Archaic period (Tuna et al., 2009; Greene et al., 2019). In the first half of the 6<sup>th</sup> c. BCE, the settlement was organized on a regular grid plan that included a network of streets and demarcation of lines of individual properties (Tuna et al., 2009). Although no material was found from the settlement’s earliest use within the presently delimited area of L1, such activity may have taken place in waters now silted within the low-lying adjacent fields, where early local and imported ceramics have been discovered; alternatively, small ships may have simply been beached rather than necessitating a quay or mole (Greene et al., 2019; Tuna et al., 2014). At the beginning of the 5<sup>th</sup> c. BCE, the settlement was reorganized and the city’s fortification system was bolstered on both land and sea, and certain indoor spaces and housing areas were rearranged to reflect the changing needs of the community (Tuna et al., 2009). Perhaps around 400 BCE, a pair of moles was added to L1 and land reclamation efforts in the adjacent seawall area expanded the harbor facilities to the east and north. To the southwest, the L2/L3 complex was built (Fig. 2), the most prominent remains of which include L2’s two well-hewn moles equipped with towers (Greene et al., 2019).

By the early Hellenistic period, there was a shift toward industrialization at Burgaz. Courtyard houses were transformed into workshops for industrial-agricultural activities including metalworking (NE and SE sectors) and weaving (SE sector), and olive oil and wine production flourished with the new Hellenistic winery (Tuna et al., 2009; Koparal et al., 2014). Rather than investing in the maintenance and expansion of the increasingly silted L1 and the L2/L3 complex, the L4 basin was developed adjacent to the winery (Fig. 2). Breakwaters were added, making for a deeper and larger inlet with shoreline installations for producing, packaging, collecting, and exporting goods (Greene et al., 2019). This activity continued into the later Roman era (Late Antiquity), as evident in what may be the remains, near the northern mole of L4, of a small 6<sup>th</sup> or 7<sup>th</sup> c. AD shipwreck (Leidwanger et al., 2015). Thus, even as Knidos flourished as the political center of the peninsula from the 4<sup>th</sup> c. BCE, Burgaz’s proximity to agricultural land and abundant space for industrial activities gave it another millennium of continued relevance in regional and interregional commerce (Greene et al., 2019; Büyüközer, 2012, 2013; Doksanaltı, 2007; Doksanaltı et al., 2016, 2018). Some of this later activity was no doubt focused on short-haul local routes, both redistribution within the Gulf of Hisarönü and by connecting the city’s storage facilities and winery with the amphora workshops and larger market center at Knidos (Leidwanger et al., 2015; Greene and Leidwanger, 2022). In contrast, Knidos mobilized this activity at Burgaz for a broader market, linking into the Aegean and the eastern Mediterranean transshipment zone.

### 3. Material and methods

#### 3.1. Stratigraphic section

Our study was conducted on sedimentary samples collected along a stratigraphic section excavated during underwater archaeological work in 2014 and 2015 within basin L1 (Fig. 2). This section, exposed in Unit P of Trench 5 (BZ.15.L1.T5.P1), was not obtained through coring but results from a stratigraphic profile documented *in situ* within a submerged excavation trench (see Fig. 7 in Greene et al., 2019). The aim was to focus on the middle and seawall edge of this earliest basin, where

several underwater archaeological trenches had been excavated in an effort to understand the shape and development of its associated coastal infrastructure. Trench 5 (T5) was divided into 7 units, each measuring 2 × 2 m (Fig. 2). The stratigraphic section studied was sampled from Unit P, located at the southern end of the trench, where the greatest depths are found near the central part of the basin. Toward this end of T5, the depths reached by the N and P units ranged from c. 2.5–3.4 m b.s.l. (Fig. 2). The stratigraphic section shows a height of 3.2 m, which is approximately 3.8 m b.s.l. (Fig. 3).

#### 3.2. Sedimentological analyses

A total of 24 samples were taken from the harbor basin deposits. The sediment fractions <2 mm were analyzed using a laser diffraction particle sizer (LS 13320, Beckman Coulter Ltd.) at the University of Cologne (Stock et al., 2016). The resulting data were then statistically analyzed using GRADISTAT (Blott and Pye, 2001). Loss-on-ignition (LOI) was measured in a muffle furnace from 10 g sediment heated for 16 h at 375 °C, and magnetic susceptibility (MS) measurements were performed with a Bartington MS2B sensor at the OMEAA technology platform (UMR 5600 and UMR 5133 CNRS) hosted at the University Lumière Lyon 2. Sedimentological data are shown in Table S1 and Fig. 3.

#### 3.3. Geochemical analyses

##### 3.3.1. Major and trace element analysis

The elemental geochemical analyses followed procedures similar to those described in Delile et al. (2014a) and are summarized briefly below. First, fine sediments (<63 µm) were separated using a nylon sieve. The samples were then digested in a mixture of concentrated double-distilled HF, HNO<sub>3</sub>, and HClO<sub>4</sub> (in a ratio of 3:1:0.5) in the clean laboratory at the Ecole Normale Supérieure de Lyon. After complete breakdown with 6M distilled HCl, the samples were re-dissolved in 2 ml concentrated distilled HNO<sub>3</sub>. Major elements were analyzed using ICP-AES (ICAP 6000), while trace elements were analyzed using Q-ICP-MS (Agilent 7500 CX). The precision for both major and trace elements ranged between 2 % and 5 %. The major and trace element data are listed in Table S1. The Pb Enrichment Factor (EF<sub>Pb</sub>) quantifies the anthropogenic contribution of Pb compared to its natural background levels (EF<sub>Pb</sub> = 1 indicates no excess of Pb). It was computed as follows:

$$EF = \frac{\left(\frac{Pb}{Al}\right)_{sed}}{\left(\frac{Pb}{Al}\right)_{bck}}$$

where sed refers to the Pb/Al ratio measured for each sediment sample of the stratigraphic section and bck refers to the local natural background value of this ratio using the deepest, and oldest, samples of the excavated section BZ.15.L1.T5.P1 (Pb ~ 5.2 ppm and Al ~ 2.4 %).

Principal Component Analysis (PCA) was conducted using Xlstat software on the major and trace element concentrations, along with loss-on-ignition (L.O.I.) and MS data sets, to decipher the main abiotic and biotic processes in the water column. This statistical analysis was conducted on the correlation matrix of standardized-transformed data sets. Each variable was centered and scaled by subtracting the mean value and dividing by the standard deviation. Eigenvalues were extracted from the resulting covariance matrix and ranked in descending order to determine the proportion of total variance explained by each component. The data were then projected into the subspace defined by the corresponding eigenvectors and typically visualized using two-dimensional or three-dimensional plots. Correlation circles from the PCA performed on major and trace element concentrations are shown in Fig. 4A.

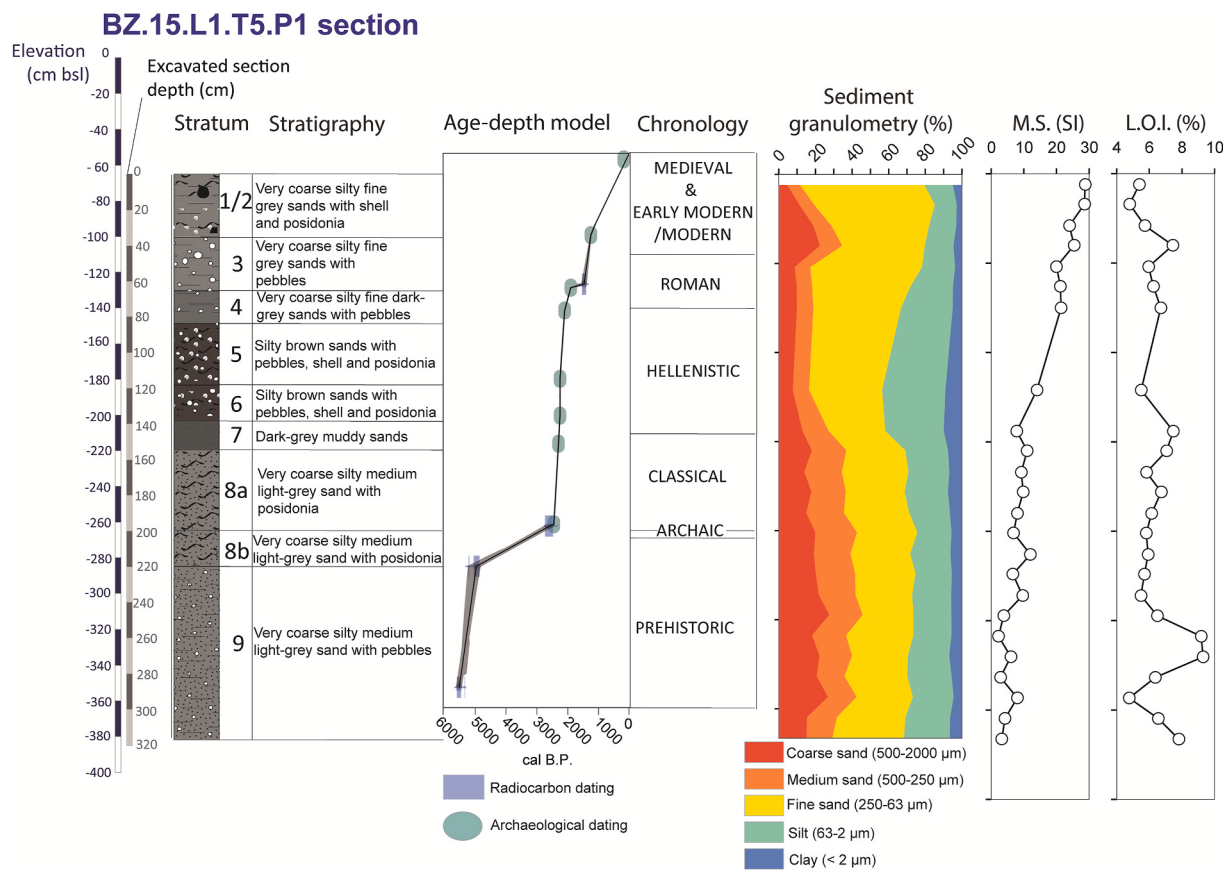


**Fig. 3.** Stratigraphic log of the L1 excavated section (L1.T5.P1) showing the age-depth model constructed using archaeological and radiocarbon dating (Greene et al., 2019), grain-size distributions, magnetic susceptibility values, and LOI content.

### 3.3.2. Pb isotope analysis

Lead isotopic compositions were measured on both leachates and residual fractions of all the sediment samples to capture the anthropogenic and natural background fingerprints of Pb, respectively. The analytical protocol is described in Delile (2014) and briefly summarized below. After splitting the sediment fraction smaller than 63 µm using a nylon sieve, an aliquot of 500 mg from each sample was leached first with hot chloroform to separate the anthropogenic Pb component, followed by hot dilute HBr, including multiple alternating ultrasonication and heating steps. After combining and evaporating to dryness the two leachate fractions, Pb was separated using anion-exchange chromatography with 1 M HBr as the eluent for the sample matrix and 6 M HCl to elute the Pb. The sample residues from the leaching procedure underwent the same acid digestion as that used for elemental concentration analysis described in §3.3.1. The Pb isotopic compositions of both the residues and leachates were measured using multi-collector inductively coupled plasma mass spectrometry (MC-ICP-MS) at the Ecole Normale Supérieure de Lyon. Thallium was added for instrumental mass bias correction, and sample-standard bracketing was performed using the values reported by Eisele et al. (2003) for NIST 981. The external reproducibility was < 100 ppm (0.01 %) for  $^{204}\text{Pb}$ -normalized ratios and < 50 ppm (0.005 %) for  $^{207}\text{Pb}/^{206}\text{Pb}$  and  $^{208}\text{Pb}/^{206}\text{Pb}$ . In-run analytical uncertainties (2SE) for both sample and standard runs were always better than the external reproducibility. The Pb isotope data and the derived geochemical parameters  $T_{\text{mod}}$  (Pb model ages in millions of years, Ma),  $\kappa$  (kappa, the  $^{232}\text{Th}/^{238}\text{U}$  ratio), and  $\mu$  (mu, the  $^{238}\text{U}/^{204}\text{Pb}$  ratio) are listed in Table S2.

### 3.3.3. Attenuated total reflectance fourier transform infrared spectroscopy (FTIR-ATR)

FTIR-ATR analysis was performed to identify the main mineral

compositions of the sediments, following the data processing methodology described by Martínez Cortizas et al. (2021) for peatlands. This methodology was recently and successfully applied to the basin deposits of Lechaion, the ancient harbor of Corinth, by Chabrol et al. (2023). We used the FT-IR Frontier Spectrometer, which includes a KBr beam splitter, a diffuse reflectance sampling accessory, and a TGS detector (PerkinElmer, Waltham, MA, USA). The mid-infrared (MIR) spectral data were measured at the Archéorient Laboratory's analytical platform (UMR 5133 CNRS, Ardèche, France). From the same sample cups used for pXRF analyses, aliquots of ~20 mg were scanned from 4000 to 380  $\text{cm}^{-1}$  with a 2  $\text{cm}^{-1}$  wavenumber spacing. To assign the mineral compositions of sediments, we compared their spectral fingerprints to those from our home-made database, which includes approximately 600 spectral references compiled from the RRUFF database (<http://rruff.geo.arizona.edu>), the Kimmel Center FTIR library (<https://centers.weizmann.ac.il/kimmel-arch/infrared-spectra-library>), and the database developed by Chapkanski et al. (2021).

The spectral infrared data in the 1600 to 380  $\text{cm}^{-1}$  range were processed using PCA with varimax rotation and a correlation matrix, operating on a transposed data matrix where wavenumbers were arranged in rows and samples in columns. The resulting observation scores matrix represented the wavenumber scores for each principal component (PC), with the aim of delineating the primary constituents of the samples. To link specific minerals or mineral species with the score spectrum of each principal component, we computed the correlation matrix between the reference spectra of minerals and the PC scores (Table S3). The most closely matched results are shown in Fig. 4B, which illustrates the PC spectra of sediment samples alongside the spectra of reference minerals. In the transposed PCA, the variable loadings matrix corresponds to the sample values for each PC. The square of the loadings, termed partial communalities, represents the proportion of the

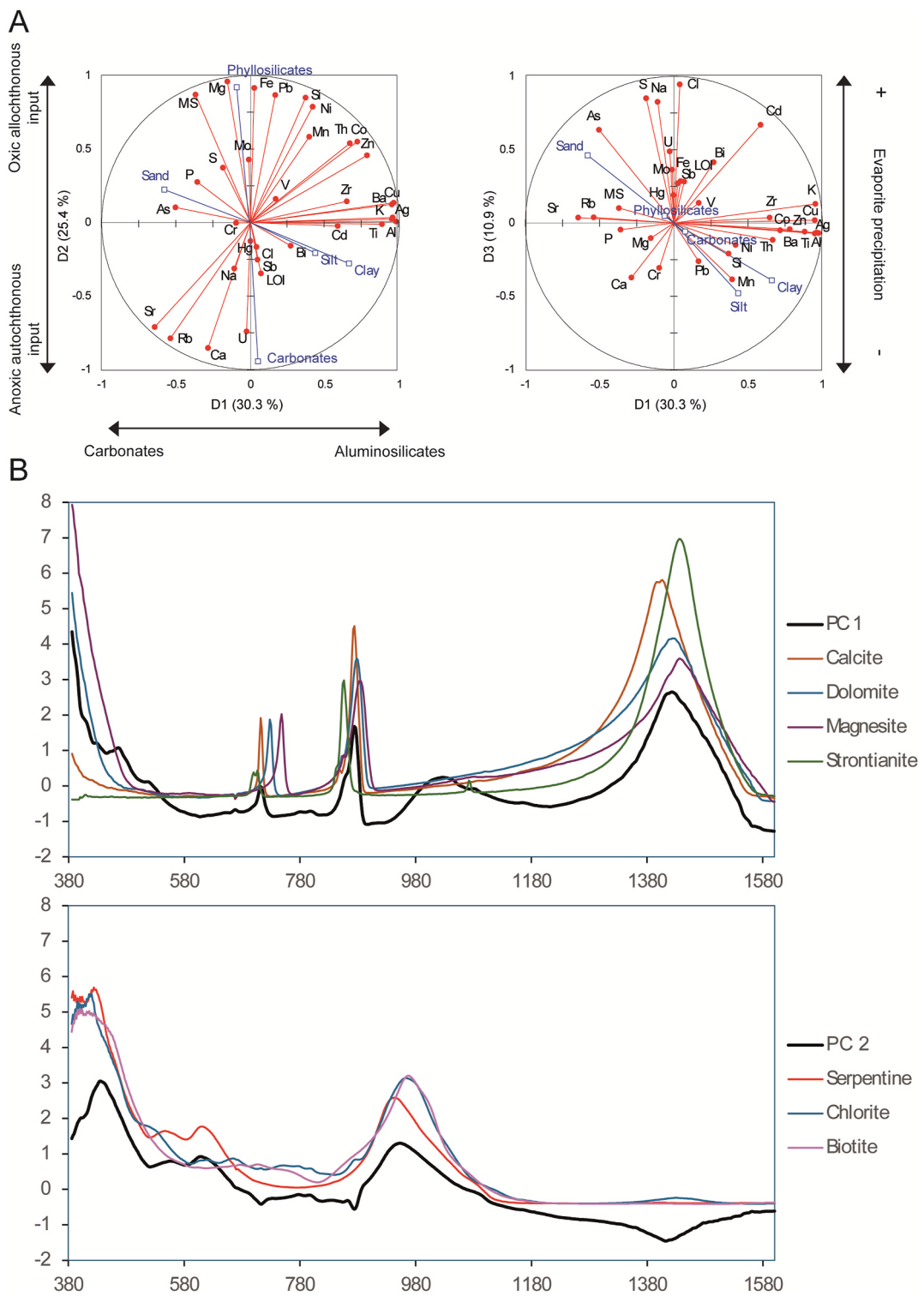


**Fig. 4.** (A) Correlation circles of the PCA for the three weightiest components (D1-D3) performed on major and trace element concentrations (red lines). Supplementary variables (blue lines) have been processed with the main mineral families and particle size classes. (B) FTIR-ATR analysis-based PCA scores of the sediment samples (black lines) and absorbance of the reference minerals (colored lines, see Table S3) with the highest loadings assigned to principal components (PC) 1 and 2. (For interpretation of the references to color in this figure legend, the reader is referred to the Web version of this article.)

sample's spectral variance explained by each component. It is assumed that stratigraphic variations in partial communalities within the sediment section indicate changes in the relative abundance of compounds or minerals (Fig. 5).

### 3.4. Radiocarbon and archaeological dating

Radiocarbon samples were selected based on the presence of organic material recovered directly from the exposed stratigraphic section. Given the ~3-m thickness of the sequence, the availability of well-preserved datable material was limited, and preference was given to

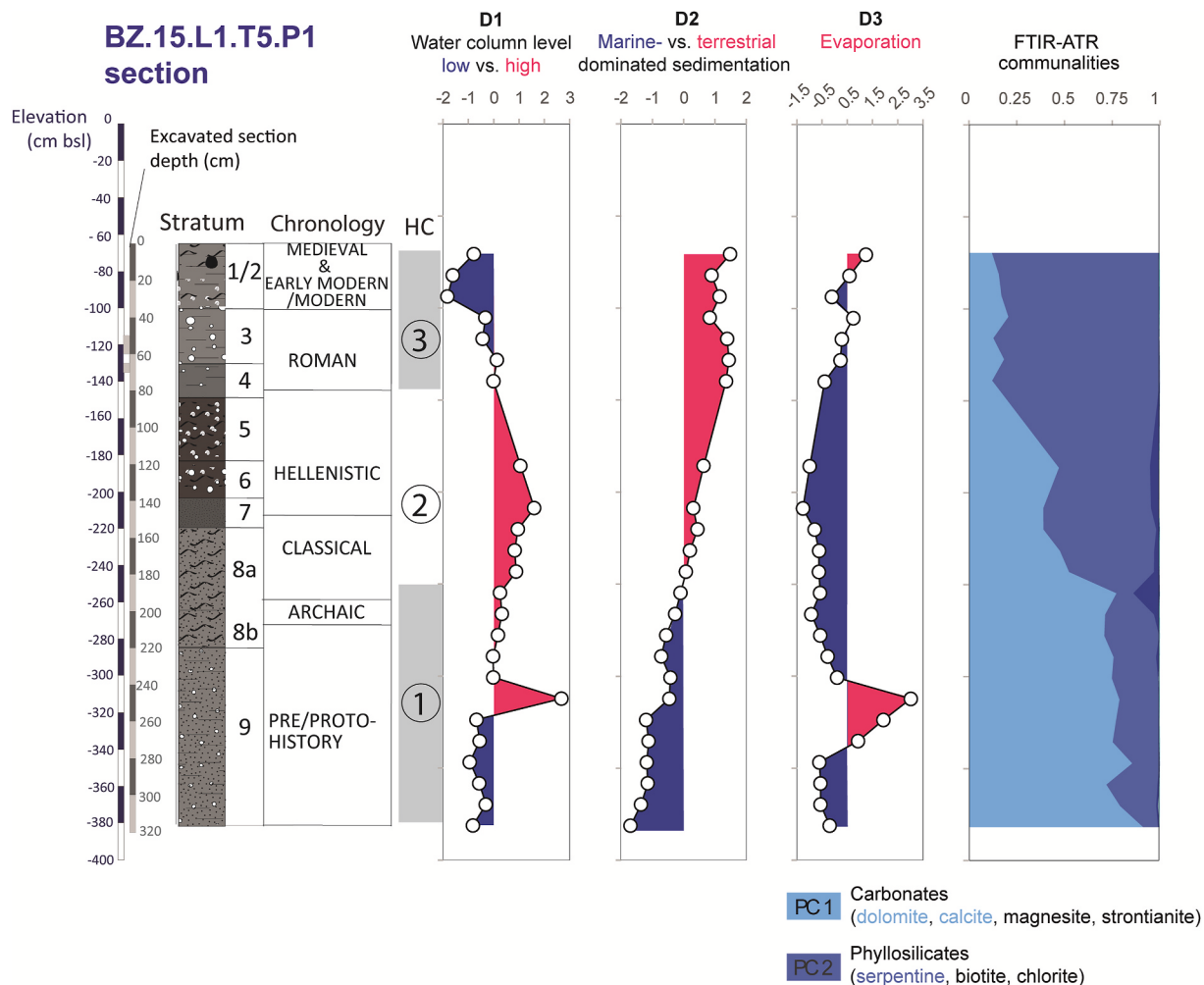


**Fig. 5.** Stratigraphic variations of PCA scores D1-D3 of major and trace element concentrations (ICP-MS-XRF) and FTIR-ATR analysis-based PCA scores of the sediment samples and loadings of the reference minerals in the principal components (PC). See Fig. 4A for correlation circles related to the PCA of major and trace element concentrations.

samples associated with secure depositional contexts and clear archaeological relevance. Four charcoal samples were AMS-<sup>14</sup>C dated (Table S4) at the Lyon Center for Radiocarbon Dating (CDRC) and calibrated using the continental curve from Reimer et al. (2020). The age-depth model of the stratigraphic section (Fig. 3) was performed using Clam software (Blaauw, 2010). In addition to radiocarbon dating, the age-depth model includes archaeologically dated materials recovered from the archaeo-stratigraphic units. The key characteristics of pottery fragments found in the harbor layers are detailed in Greene et al. (2019). To facilitate temporal interpretation across the figures and ensure consistency with both stratigraphic units and archaeological context, a pragmatic chronological framework was adopted. The periods were defined as follows.

- Pre-/Protohistory (before the 8<sup>th</sup> c. BCE)
- Archaic (8<sup>th</sup>–early 5<sup>th</sup> c. BCE)
- Classical (early 5<sup>th</sup>–late 4<sup>th</sup> c. BCE)
- Hellenistic (late 4<sup>th</sup>–mid-2<sup>nd</sup> c. BCE)
- Roman (mid-2<sup>nd</sup> c. BCE to mid-7<sup>th</sup> c. AD [including Late Antiquity, ~4<sup>th</sup>–mid-7<sup>th</sup> c.])
- Medieval and Early Modern/Modern (mid-7<sup>th</sup>–present)

The transition date selected between the Hellenistic and Roman periods reflects the gradual consolidation of Roman political and economic control over the eastern Mediterranean from the mid-2<sup>nd</sup> c. BCE

onward. This chronological framework was adapted according to the requirements of each figure. Accordingly, the Roman to Modern periods are treated as a single group, while the Archaic, Classical, and Hellenistic periods are collectively referred to as the Greek period (Archaic to Hellenistic).

## 4. Results

### 4.1. FTIR spectra

As indicated in the materials and methods, PCA was applied to FTIR spectral data from the sediment samples and our in-house reference mineral spectral database to assess the mineral compositions of the sediments. The first two of the five PCs account for 55 % of the MIR spectral signal (Table S3) and, once transposed in partial communalities, the spectral variance of the samples explained by PC1 and PC2 averages >98 % (Fig. 5). Correlations greater than 0.7 between the reference minerals and the five PCs are shown in Table S3, with their MIR spectral range plots displayed against those of PC1 and PC2 in Fig. 4B. The MIR spectral signals of PC1 and PC2 correspond closely to carbonate and phyllosilicate minerals, respectively. Calcite and dolomite align more precisely with the shape of the PC1 MIR signal, while serpentine strongly matches the spectral signature of PC2.

Fig. 5 shows the stratigraphic distribution of the FTIR-ATR communalities, which should not be considered as a quantitative

measurement of mineral content, but rather as an indication of relative changes in their abundance. From the bottom of the BZ.15.L1.T5.P1 stratigraphic section, at a depth of 3.85 m b.s.l., up to 2.55 m b.s.l., carbonates largely prevail, accounting for an average of 71 % ( $\pm 8\%$ ) of the MIR spectral variance, while phyllosilicates represent only 25 % ( $\pm 8\%$ %). Sands are the main granulometric carrier of carbonates, representing an average of 72 % ( $\pm 2\%$ ), while silts and clays contribute 22 % ( $\pm 2\%$ ) and 6 % ( $\pm 1\%$ ), respectively (Fig. 3). In the upper part of the stratigraphic section, from 2.55 to 0.71 m b.s.l., the mineralogical ratio shifts drastically in favor of a steady increase in phyllosilicates (mean value of 73 %  $\pm 12\%$ ) and a decrease in carbonates (mean value of 26 %  $\pm 11\%$ ) (Fig. 5). Unexpectedly, this reversal in the mineralogical content is not reflected in the granulometry of the upper deposits, as the proportions of sand, silt, and clay remain consistent at 72 % ( $\pm 9\%$ ), 22 % ( $\pm 7\%$ ), and 6 % ( $\pm 2\%$ ), respectively (Fig. 3).

#### 4.2. Geochemical reservoirs

The identification of the main geochemical reservoirs, which helps to discriminate between or determine the processes and environmental variables involved in the formation of sediment deposits, was based on PCA with varimax rotation, as described by Martín-Puertas et al. (2011), Delile et al. (2018) and Bertrand et al. (2024). This statistical treatment was conducted on the data of thirty trace and major elements, MS, and L. O.I. Supplementary variables, which do not influence the coordinates of the active ones, were added to facilitate the interpretation of the principal components. These supplementary variables include the granulometric classes and the PC1 and PC2 communalities. Using this method, three main components (D1, D2, and D3), which together account for 68.5 % of the total variance in the geochemical dataset, were identified. Although the cumulative variance of the first three components falls slightly below 70 %, this value is consistent with similar geoarchaeological studies of ancient harbor sediments, where the average cumulative variance typically ranges from 60 % to 80 % (Delile et al., 2014a, 2015, 2016a, 2018; Chabrol et al., 2023). Following standard recommendations in environmental geochemistry (Albarède, 1995; Reimann et al., 2008), we retained only the components whose individual contribution to total variance exceeds  $\sim 10\%$ , thus avoiding the risk of overinterpreting statistical noise. Fig. 4A shows the correlation circles of the PCA, where the weights of the variables (loadings) are displayed for each of the three principal components in order of importance.

- 1) The first factor D1 (30.3 % of the total variance) exhibits positive loadings for Al, Ti, K, Ba, Zr, Ag, and Cu, and negative loadings for Sr, As, and Rb, which reflect the aluminosilicate detrital fraction as opposed to the carbonate fraction. This opposition is common, as it reflects fine clay minerals on one side and coarse carbonate sediments on the other. The strong association of clay and sand variables with the D1 axis supports this observation. This pattern was also identified in the factorial axes F2 of the harbor deposits at Ostia (Delile et al., 2018), F1 at Portus (Delile et al., 2014a), F3 at Neapolis (Delile et al., 2016a), and F1 at Ephesus (Delile et al., 2015) and Lechaion (Chabrol et al., 2023). D1 scores split Burgaz's harbor basin sediments into three parts (Fig. 5). Carbonate sands prevail in the lower (3.8–3.2 m b.s.l.) and upper (1.4–0.7 m b.s.l.) sections, while clay minerals dominate in the intermediate section (3.2–1.4 m b.s.l.).
- 2) The second factor D2 accounts for 25.4 % of the total variance. Positive loadings highlight another group of detrital elements (Si, Th, Mg, Pb, Ni, Co), most likely tied with phyllosilicate minerals, as well as elements that precipitate in oxic environments, such as Fe and Mn hydroxides and MS. Serpentine is the mineral phase that carries this group of detrital elements, as these hydrated magnesium silicate minerals primarily consist of Mg and Si, and also contain minor amounts of Fe, Mn, Ni, and Cr. For this reason, we consider this component to be an oxic allochthonous input, contrasting with the

anoxic autochthonous input shown in the D2 negative loadings. Indeed, Sr- and Ca-rich sediments are often associated with biological processes, such as the formation of skeletons and shells by marine organisms such as foraminifera, corals, and mollusks. Biogenic calcite and dolomite can form from the remains of these organisms. Uranium-rich sediments indicate anoxic conditions where dissolved uranium is reduced from U(VI) to U(IV) and precipitates. As a result, the D2 negative component records autochthonous biogenic carbonate formation. D2 scores divide the Burgaz harbor basin sediments into two approximately equal parts: anoxic autochthonous-dominated sedimentation from 3.80 to 2.55 m b.s.l., which is gradually replaced by oxic allochthonous inputs up to the top of the stratigraphic section (Fig. 5).

- 3) The third factor D2 represents for 10.9 % of the total variance. High levels of Na and Cl in a thin layer at approximately 40 cm m b.s.l. (3.5–3.1 m b.s.l.) (Fig. 5) suggest that these marine-dominated elements reflect high evaporation rates, leading to the precipitation of evaporite minerals like halite (NaCl). Such a process coincides with a shift in redox conditions, as indicated by the increase in S, As, Cd, and U under reducing and anoxic (low oxygen) environments.

Based on the PCA scores from D1, D2, D3, and PC1 and PC2 communalities, a Hierarchical Clustering (HC) was performed, identifying three units (HC 1–3) in Fig. 5 that broadly correspond to major chronological phases: HC 1 for Pre/Protohistory, HC 2 for the Greek periods (Archaic to Hellenistic), and HC 3 for Roman to Modern times.

#### 4.3. TME concentrations and Pb isotopes

Fluctuations in the Enrichment Factor (EF) values of trace metal elements (TME) throughout the stratigraphic section are shown in Fig. 6. A threshold value of 1.5 was used to indicate anthropogenic enrichment. Any value less than or equal to 1.5 is regarded as natural. All TME show EF values lower than or equal to this threshold ( $EF_{Ag} = 1.1 \pm 0.1$ ,  $EF_{Hg} = 1.0 \pm 0.6$ ,  $EF_{Cu} = 1.1 \pm 0.1$ ,  $EF_{Zn} = 1.1 \pm 0.1$ ,  $EF_{As} = 0.9 \pm 0.5$ ,  $EF_{Cd} = 1.1 \pm 0.4$ ,  $EF_{Sb} = 1.0 \pm 0.4$ ,  $EF_{Cr} = 0.9 \pm 0.3$ ,  $EF_{Ni} = 1.2 \pm 0.2$ ,  $EF_{Co} = 1.3 \pm 0.3$ ), except for Pb (mean value  $1.9 \pm 0.8$ ). Its profile within the stratigraphy splits three levels from the base to the top: from 3.8 to 2.8 m b.s.l.  $EF_{Pb} = 1.1 \pm 0.8$ , from 2.7 to 2.1 m b.s.l.  $EF_{Pb} = 1.9 \pm 0.2$ , and from 1.9 to 0.7 m b.s.l.  $EF_{Pb} = 2.9 \pm 0.3$  (Fig. 6 and Table S2).

The Pb isotopic compositions of both the residual and leachate fractions of the sediments provide an effective means of distinguishing the natural from the anthropogenic component. Residual or crustal Pb is found within the crystalline lattice of the mineral matrix in the sediments, carrying an isotopic fingerprint that reflects the local geological environment, that is, a mix of different sedimentary sources. Meanwhile, leachate Pb is adsorbed onto sediment carrier phases that bind Pb emitted from exogenous sources, particularly anthropogenic ones. Although Pb is a hydrophobic micropollutant, some Pb is present in dissolved form and, under certain conditions, can precipitate onto carrier phases. This is why leached Pb reflects a mixture of both natural and anthropogenic sources. Fig. 6 also highlights the stratigraphic profiles of leachate  $^{206}Pb/^{204}Pb$ ,  $^{207}Pb/^{204}Pb$ , and  $^{208}Pb/^{204}Pb$  isotopic ratios, as well as the geochemically informed parameters  $T_{mod}$  (Pb model age in millions of years, Ma),  $\kappa$  (the  $^{232}Th/^{238}U$  ratio), and  $\mu$  (the  $^{238}U/^{204}Pb$  ratio). Readers interested in more information on the use of these parameters can refer to the following articles: Albarède et al. (2012) for computing parameters, Blichert-Toft et al. (2016) for tecto-structural insights, Albarède et al. (2016, 2020, 2021, 2024a,b, 2025) for archaeometric applications, and Delile et al. (2014b, 2015, 2016b, 2017, 2019) for geoarchaeological applications.

The Pb isotopic compositions show minor variations within the sediment profile, with values ranging from 38.676 to 38.891 (mean  $38.855 \pm 0.050$ ) for  $^{208}Pb/^{204}Pb$ , from 15.664 to 15.688 (mean  $15.680 \pm 0.005$ ) for  $^{207}Pb/^{204}Pb$ , and from 18.611 to 18.826 (mean  $18.791 \pm 0.049$ ) for  $^{206}Pb/^{204}Pb$ . The main signal variations occur within the

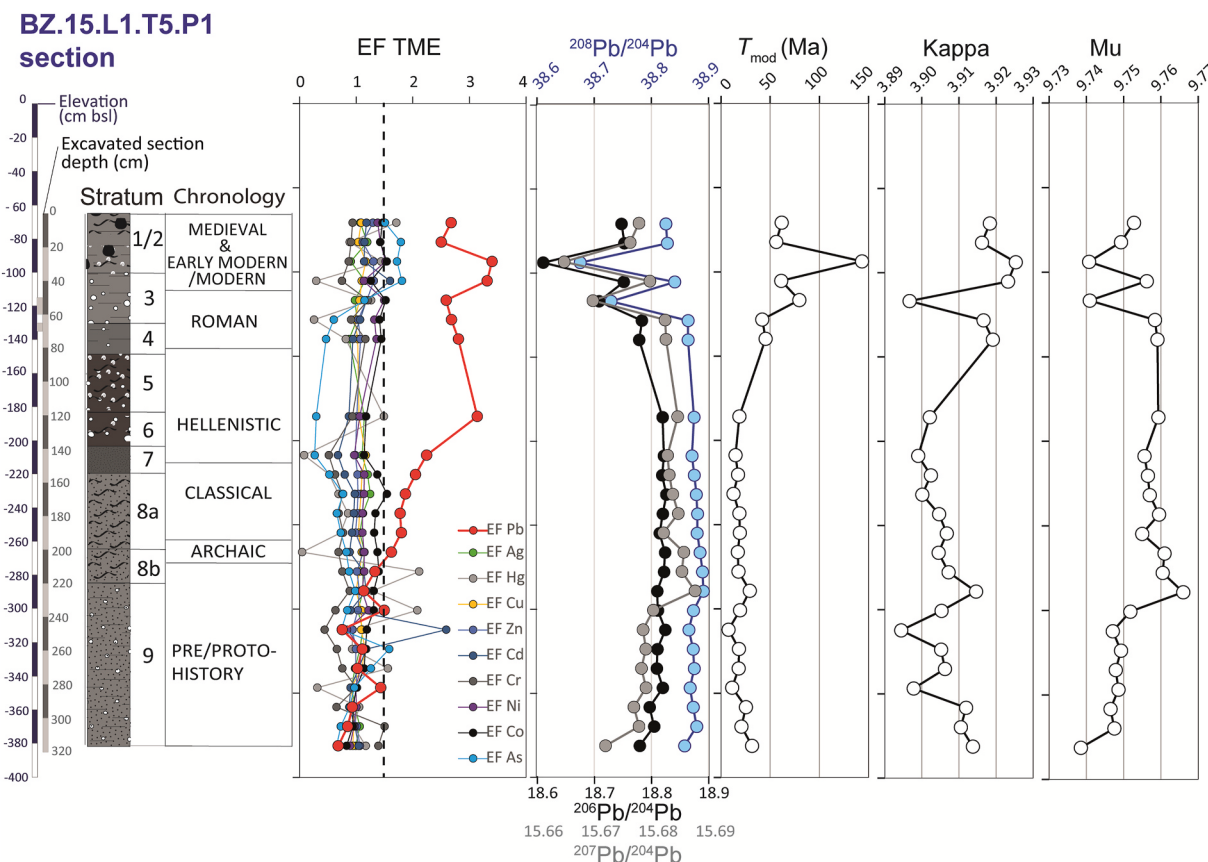


**Fig. 6.** Stratigraphic variations in the Enrichment Factor (EF<sub>Pb</sub>) of trace metal elements,  $^{208}\text{Pb}/^{204}\text{Pb}$ ,  $^{206}\text{Pb}/^{204}\text{Pb}$ ,  $^{207}\text{Pb}/^{204}\text{Pb}$ ,  $T_{\text{mod}}$ , kappa ( $\kappa$ ,  $^{232}\text{Th}/^{238}\text{U}$ ), and mu ( $\mu$ ,  $^{238}\text{U}/^{204}\text{Pb}$ ).

upper 1.2 m b.s.l. of the sediment section. The geochemically informed parameters derived from the measured Pb isotope compositions provide enhanced clarity due to their much broader value ranges: from 7.6 to 143.3 (mean value  $33.6 \pm 30.0$ ) for  $T_{\text{mod}}$ , from 9.739 to 9.766 (mean value  $9.753 \pm 0.007$ ) for  $\mu$ , and from 3.894 to 3.925 (mean  $3.908 \pm 0.009$ ) for  $\kappa$  (Fig. 6).

The stratigraphic evolution of the Pb isotopic compositions shows two trends. The parameters  $T_{\text{mod}}$  and  $\kappa$  ( $r = 0.6$ ) describe a pattern similar to that of the measured Pb isotope ratios, with a notable break at the top of the sediment section where the model ages are  $>50$  Ma between 0.7 and 1.2 m b.s.l. and  $\kappa > 3.915$  between 0.7 and 1.4 m b.s.l. (Fig. 6). The parameter  $\mu$ , on the other hand, splits three distinct levels: ~9.75 from 3.0 to 3.8 m b.s.l., ~9.76 from 3.8 to 1.2 m b.s.l., and from 9.74 to 9.75 from 1.2 to 0.7 m b.s.l. With a few exceptions (samples 2.89 m and 2.78 m), the  $T_{\text{mod}}$  vs  $\mu$  and  $\kappa$  vs  $\mu$  plots highlight three groups of samples corresponding to the chronological periods Pre/Protohistoric, Greek (Archaic to Hellenistic), and Roman to Modern (Fig. 7). Indeed, the threshold value of approximately 9.75 for  $\mu$  differentiates the Pre/Protohistory group (lower values) from the Greek group (higher values). The parameters  $T_{\text{mod}}$  and  $\kappa$  distinguish the Roman to Modern group from the other two clusters based on threshold values of approximately 40 Ma and 3.915, respectively (Fig. 7).

## 5. Discussion

### 5.1. Dual control of sedimentation rhythms

To characterize the palaeo-environmental evolution within the harbor basin, it is necessary to first compare the chronostratigraphy of the sedimentary deposits with Holocene sea level rise. Fig. 8 shows the age-depth model of the sediment samples alongside Holocene relative sea

level (RSL) curves at both local (Datça Peninsula; Kayan, 1988) and regional (eastern Aegean Sea; Vacchi et al., 2014) scales. The age-depth model ages of the sediment samples align remarkably well with the general shape of that of the Aegean sector "C" (Fig. 8). Indeed, sediment aggradation rates of the Burgaz harbor basin's seafloor are divided into three distinct phases, two of which show similar trends to sea level rise rates in the Aegean Sea.

- 1) From 5702 to 4967 cal BP, seafloor aggradation was  $1.25 \text{ mm.yr}^{-1}$  and sea-level rise  $1.90 \text{ mm yr}^{-1}$ ;
- 2) From 2589 to 2054 cal BP, seafloor aggradation was  $2.35 \text{ mm.yr}^{-1}$  and sea-level rise  $0.54 \text{ mm yr}^{-1}$ ;
- 3) From 1468–587 cal BP, seafloor aggradation was  $0.65 \text{ mm.yr}^{-1}$  and sea-level rise  $0.52 \text{ mm yr}^{-1}$ .

This segmentation exhibits a stair-step shape (Fig. 8), indicative of sedimentary hiatuses characteristic of past dredging operation marks. Such traces have been found in many parts of the Mediterranean, including Tyre (Marriner and Morhange, 2006), Sidon (Marriner et al., 2006), Ephesus (Kraft et al., 2000; Delile et al., 2015; Stock et al., 2016), Neapolis (Marriner and Morhange, 2006; Carsana et al., 2009; Delile et al., 2016a), Utica (Pleuger et al., 2019), Portus (Salomon et al., 2016; Lisé-Pronovost et al., 2019), and Ostia (Goiran et al., 2014; Salomon et al., 2016). A first dredging operation, with a chronological gap of approximately 2500 years, is believed to have occurred around 2600 cal BP (2473–2733 cal BP) at the time of the foundation of Burgaz around 700 BCE (Tuna et al., 2009). Although no direct architectural evidence of dredging survives from this period, the stratigraphic hiatus and sudden increase in aggradation rates around 2600 cal BP suggest that the basin may have been intentionally deepened or expanded to serve emerging harbor functions. Following the methodology developed by

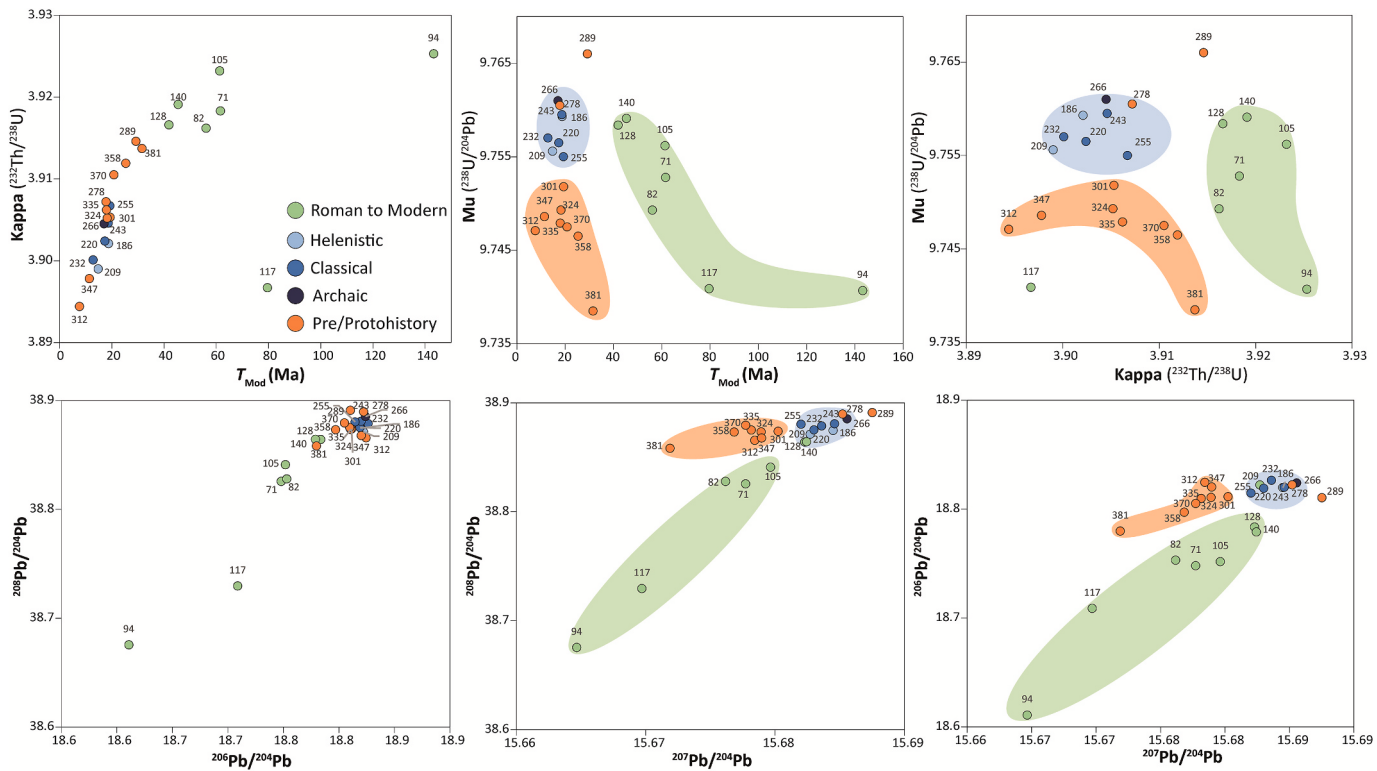


**Fig. 7.**  $T_{\text{mod}}$  vs kappa,  $T_{\text{mod}}$  vs  $\mu$ ,  $\kappa$  vs  $\mu$ ,  $^{206}\text{Pb}/^{204}\text{Pb}$  vs  $^{208}\text{Pb}/^{204}\text{Pb}$ ,  $^{207}\text{Pb}/^{204}\text{Pb}$  vs  $^{208}\text{Pb}/^{204}\text{Pb}$ , and  $^{207}\text{Pb}/^{204}\text{Pb}$  vs  $^{206}\text{Pb}/^{204}\text{Pb}$  for sample leachates. Colored ellipses represent the Pre/Protohistory period (orange), the Greek period (Archaic to Hellenistic in blue), and the Roman to Modern periods (green), as defined by the radiocarbon and archaeological dating-based age-depth model. (For interpretation of the references to color in this figure legend, the reader is referred to the Web version of this article.)

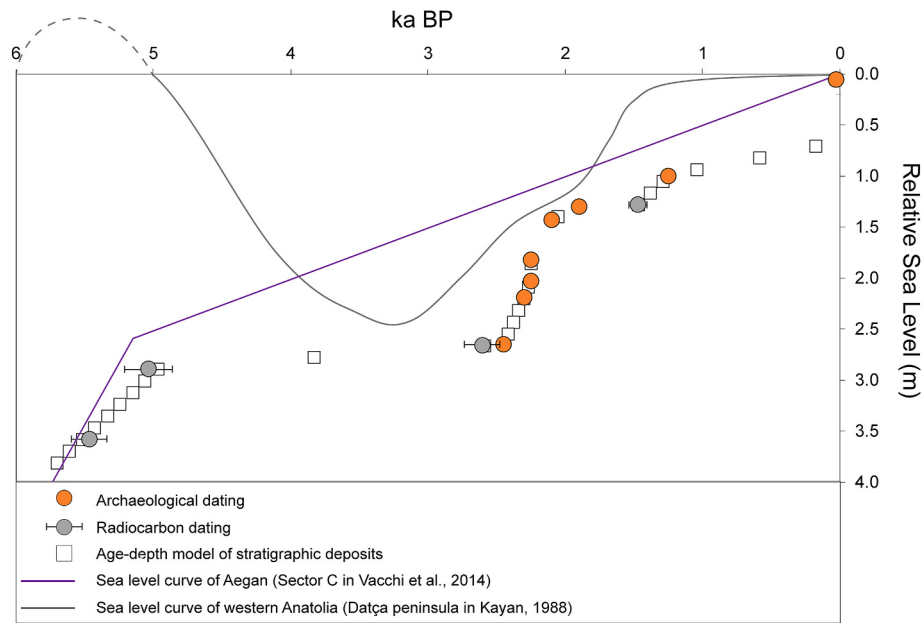


**Fig. 8.** Sea-level curves of the eastern Mediterranean (gray and purple lines) plotted with  $^{14}\text{C}$  (grey circles) and archaeological (orange circles) dating, and the age-depth model of harbor deposits (white squares). (For interpretation of the references to color in this figure legend, the reader is referred to the Web version of this article.)

Salomon et al. (2016) for the harbor basins of Ostia and Portus, Seeliger et al. (2017) compared the water column heights of the harbor basins of Elaia (Western Türkiye) with the drafts of the major warships from the period in order to assess changes in harbor usage over time. Applied to Burgaz's L1 basin, the ship draught of  $\sim 1.4$  m between the 8<sup>th</sup> and 6<sup>th</sup> c.

BCE suggests that the most prevalent class of warships (Morrison and Coates, 1986, 1996) — i.e., the trireme (minimal navigable depth of  $\sim 1.1$  m) — could have moored in the port. However, the larger warships that would come to dominate navies of the late Classical and Hellenistic periods, which required minimal navigable depths of  $>1.5$  m, could not

have moored, nor could the larger merchant ships of the Hellenistic and early Roman periods (minimal navigable depth of <2.0 m) (Boetto, 2010; Auriemma and Solinas, 2009).

A second dredging operation appears to have occurred in Late Antiquity, around the 5<sup>th</sup>-6<sup>th</sup> c. AD (chronological gap ~500 years) (Fig. 8). It occurred after a very high sedimentation phase between 2589 and 2054 cal BP, which likely threatened whatever harbor activities were still being carried out during the Roman period. Indeed, around 100 BCE, the water depth was no more than ~30 cm, effectively prohibiting activities for the vast majority of ships. Among the other operations undertaken to ensure continued maritime access at Burgaz, the new larger L4 basin was developed further north and integrated with L1 by the seawall during the 3<sup>rd</sup> and 2<sup>nd</sup> c. BCE (Fig. 2) (Greene et al., 2019). In addition to the rapid silting of L1, the growth of Hellenistic Burgaz was perhaps based on its ability to develop a dual port system along the Datça Peninsula with Knidos, particularly through its new L4. Serving effectively as Knidos's offsite hub for storage and shipment, Burgaz was able to continue distributing goods from its hinterland through Knidos by sea and probably also by land (Greene and Leidwanger, 2019, 2022). Although L4 could have definitively replaced L1 due to its larger size and ability to accommodate deeper vessels, the second dredging operation in L1 during Late Antiquity suggests that it continued to serve at least smaller ships with a draught of only 0.5–0.6 m (Fig. 8). These two harbors could then have operated in tandem throughout antiquity, as evidenced by finds from as late as the 6<sup>th</sup> c. AD and a small shipwreck from this period recorded in the shallows of L4 (Leidwanger et al., 2015; Greene et al., 2019).

This phase of rapid seafloor aggradation of the harbor basin, spanning from the 7<sup>th</sup> c. BCE to the 5<sup>th</sup> c. AD, stands out from the pre- and post-harbor stages, which are characterized by a calibration of the seafloor aggradation rate to the pace of sea level rise. Indeed, the parallelism between the sea level rise curve for the Aegean Sea and the alignment of age-depth models of stratigraphic deposits is striking (Fig. 8). Our underwater observations on the geometry of late Quaternary depositional sequences along the southern edge of the Datça Peninsula reveal a thin Holocene sandy layer overlaying oblique or subparallel rocky ridges to the coast. These ridges are composed of numerous conglomerate and sandstone banks from the Pliocene basin, with a few outcrops scattered across the seafloor. These shoals are clearly visible up to 200–300 m from the shore, forming a gentle slope seaward. These geomorphological conditions thus limit the available accommodation space needed for the accumulation of thick, shallow deposits. Their development is further constrained by the weak influence of coastal progradation or retrogradation processes, largely due to coastal erosion. With the beach profile in equilibrium, the accretion of the seafloor developed vertically beneath a water depth of ≤50 cm (tidal zone or wave run-up), the rate being controlled by sea level rise in the absence of human intervention such as dredging.

## 5.2. Holocene palaeo-environmental evolution

### 5.2.1. Palaeo-environmental processes

The Hierarchical Clustering (HC) performed on PCA scores derived from the geochemical data and FTIR-ATR spectral communalities delineates three typical stratigraphic harbor sequences (HC 1–3 in Fig. 5), corresponding to the pre-harbor phase (pre-limenic unit) during the Pre-/Protohistoric era, the harbor phase (limenic unit) during the Greek periods (Archaic to Hellenistic), and the post-harbor phase (meta-limenic unit) during the Roman to Modern periods (Goiran and Morhange, 2003; Goiran et al., 2022). Each of these major units displays distinct physico-chemical properties, which are reflected in variations in the relative contributions of the geochemical reservoirs (cf. § 4.2. and Fig. 4A and 5). The palaeo-environmental processes linked to these geochemical reservoirs are outlined below.

- 1) D1 scores are interpreted as an indicator of variations in water column height, with a dominated carbonate fraction at lower levels and a dominated aluminosilicate detrital fraction at higher levels. Such an interpretation has been reported by Martín-Puertas et al. (2011) for the Zōnar Lake (Spain) level variations, where Sr-rich sediments are contrasted with sediments enriched in aluminosilicate-bound elements such as Al, K, and Ti. The alternation between higher and lower water-column height phases perfectly matches those identified above in the seafloor aggradation rhythms (see phases 1 to 3 in § 5.1.), for which the gap with the sea level rise curve determines the water-column height (Fig. 8).
- 2) The negative D2 scores track anoxic autochthonous sediments that indicate weak column ventilation and the presence of biogenic calcite and dolomite shell remains. The prevalence of these two environmental parameters in coastal sedimentary records indicates a marine environment (Tribouillard et al., 2006; Delile et al., 2016a, 2018; Riddick et al., 2022) that is well protected from currents and waves. Conversely, the positive D2 axis values record oxic allochthonous elements, most likely related to a serpentine-carrier mineral phase originating from inland terrigenous inputs derived from the Plio-Quaternary Datça basin infill (Dirik, 2007; Özsayın et al., 2021).
- 3) Positive D3 scores reflect marine-dominated elements that precipitate due to high evaporation rates. Increased salinity from drier conditions and/or lower water-column depth leads to higher concentrations of these elements. Typically, such conditions are also accompanied by an increase in sulfur due to reduced oxygen (anoxia) (Martín-Puertas et al., 2011; Delile et al., 2016a).

### 5.2.2. Palaeo-environmental reconstitution

The pre-harbor phase (HC1, 3.8–2.7 m b.s.l.) corresponds to coastal marine sediments devoid of cultural material (Greene et al., 2019), dated to the 6<sup>th</sup> mil. cal. BP and characterized by negative D2 scores (Fig. 5). This unit can be subdivided into two phases: from 3.8 to 3.2 m b.s.l., low D1 values indicate a very shallow coastal bay, whereas between 3.2 and 2.7 m b.s.l., a deepening trend is evidenced by positive D1 values and an increasing discrepancy between the modeled sediment depths and the Aegean sea-level curve (Fig. 8). These features suggest a marine transgression that shaped the initial harbor environment between ~5300 and 5100 cal BP. A peak in D3 scores and associated marine elements (LOI, Na, Cl, S, U) may indicate an evaporative episode, inconsistent with the highstand sea level of ~+0.5 m a.s.l. proposed by (Kayan, 1988; Fig. 8) and with the inferred inland extent of the Holocene transgression. More broadly, this phase aligns with regional transgressive episodes documented at Abdera on the Thracian coast and at Liman Tepe in Izmir Bay, which similarly shaped Aegean coastal landscapes during the mid-Holocene (Mayoral et al., 2024; Riddick et al., 2022).

As noted above, the harbor phase (HC2, 2.7–1.4 m b.s.l., Fig. 5) follows a major physical disturbance in the stratigraphy, linked to the removal of ~2500 years of sediment during the initial excavation of the Burgaz harbor basin around the mid-7<sup>th</sup> c. BC. This hiatus, likely intended to accommodate greater ship drafts, is reflected in the positive D1 values, indicating a higher water column. With the commissioning of enclosing walls during the Classical period acting as an efficient trap, sedimentation rates roughly doubled while sea-level rise slowed significantly, resulting in rapid siltation (Greene et al., 2019). Further evidence of such harbor engineering is found east of basin L1 (Fig. 2), where redeposited ceramics behind the seawall connecting L1 and L4 suggest erosion control efforts to maintain port access (Greene et al., 2019; Wilker et al., 2019). A second, anthropogenic factor driving sediment input relates to Burgaz's role as an agricultural hub. Expansion of arable land during the Hellenistic demographic boom almost certainly enhanced erosion (Kayan, 1988; Greene and Leidwanger, 2019; Alcock, 1993; Sakarya et al., 2019), a trend widely recognized in ancient Mediterranean harbors (Marriner and Morhange, 2007; Stock et al., 2016;

Giaime et al., 2019). This intensification is evidenced by rising D2 scores and increasing serpentine content (Fig. 5). The post-harbor phase (HC3, 1.4–0.7 m b.s.l.) follows a second dredging operation around the late 5<sup>th</sup> c. AD, likely intended to preserve minimal draft conditions for small vessels into Late Antiquity. While archaeological surveys point to a gradual shift in port activity toward basin L4 from the Hellenistic period onward (Leidwanger et al., 2015; Greene et al., 2019), some limited use of L1 likely continued, forming part of a complementary harbor system. Due to the low resolution of the age-depth model, it is difficult to assess how long L1 remained in use after this second dredging. However, the draught from the medieval to Modern periods (~30 cm) was likely insufficient for most vessels (see D1 axis in Figs. 5 and 8). Positive D2 scores reflect persistent terrestrial input, while decreasing D3 values point to intensifying evaporitic and eutrophic conditions (Fig. 5). Such environmental transitions are common in abandoned harbor settings, as documented at Ephesus, Lechaion, and the Trajanic basin at Portus (Delile, 2014; Delile et al., 2014a, 2015; Riddick et al., 2021; Chabrol et al., 2023).

### 5.3. Pb-related human impact

#### 5.3.1. Chronology of the Pb content enrichment

Among the ten TME measured, only Pb shows excessive values associated with anthropogenic emissions ( $EF_{Pb} \geq 1.5$ ). Concentrations of the other TME remain within the range of natural background levels ( $EF_{TME} \pm 1$ ) (Fig. 6). This suggests that the archaeomaterial source of contamination is primarily, if not exclusively, composed of this metal. Conversely, the association of other TME in excess with Pb could indicate a contamination source from one or more alloys (Elmaleh et al., 2012), mining activities (Cooke et al., 2007; Delile et al., 2019; Ortiz et al., 2021; Guédon et al., 2021), metalworking (Younes et al., 2024), or several unidentified urban sources (Holdridge et al., 2021). At Burgaz, it is not surprising to observe a potential source containing only Pb, given that objects made from this metal for maritime purposes were found during underwater archaeological investigations in and around L1. In this regard, Greene et al. (2019) report, among the metal objects, pieces of lead sheathing likely from ship hulls, as well as a lead anchor core from the Classical or early Hellenistic period. Complementary compositional analyses of metal artifacts from the settlement at Burgaz also indicate the local use of Pb-based materials, especially since the Classical period (Kaptan, 2003), providing material evidence of lead circulation and processing within the site. In line with this, the source of Pb is likely to have been the Hellenistic-Roman metal workshops at Burgaz along the L1–L4 coastal area, as well as earlier residential quarters abandoned following the mid-4<sup>th</sup> c. BCE shift on the peninsula (Tuna et al., 2009).

$EF_{Pb}$  values distinctly differentiate three chronostratigraphic units:  $EF_{Pb} \sim 1$  in the Pre/Protohistoric era,  $EF_{Pb} \sim 2$  in the Archaic and Hellenistic periods and  $EF_{Pb} \sim 3$  in the Roman to Modern periods (Fig. 6). According to Sutherland's (2000) classification of  $EF_{TME}$ , which is based on urban stream sediments <63 µm,  $EF_{TME}$  values ~2 indicate minimal pollution, while those between 2 and 5 represent moderate pollution. This low to moderate anthropogenic Pb excess, ranging from 0.7 to 3.4, is similar to the values for copper ( $EF_{Cu} \sim 0.3\text{--}3.7$ ) measured by Younes et al. (2024) in the fluvial archives of Khufu's harbor at Giza (Egypt) between 7000 and 3000 BP. In some cases, TME palaeo-pollution trapped in this type of sedimentary environment is likely to provide evidence of human occupation predating the purported foundation of the site. The most iconic example concerns Alexandria, where Pb excesses recorded in the deposits of the Maryut lagoon and Alexandria Bay, dating back to the Predynastic period between 3800 and 3500 BCE, challenge the widely accepted assumption that the city was created *ex nihilo* by Alexander the Great in 334 BCE (Goiran, 2001; Véron et al., 2006, 2013).

At Burgaz, highlighting human occupation prior to the city's foundation is challenging because the first dredging operation seemingly

removed sedimentary archives of interest. Nevertheless, the geochemical content of the initial harbor sediments shows a discrete first phase of Pb contamination in the mid-7<sup>th</sup> c. BCE (2.7 m b.s.l.) (Fig. 6), probably associated with the initial phase of the city's occupation starting in the 8<sup>th</sup> c. BCE (Tuna et al., 2009) which continued into the Classical period. During this period, a steady increase in contamination was recorded, with  $EF_{Pb}$  values rising gradually from 1.6 to 2. This trend could be the hallmark of the city's development and evolution, which was characterized by the structuring of the urban fabric in the 6<sup>th</sup> c. BCE (Tuna et al., 2009), as well as the enlargement of L1 and the foundation of L2 and L3 probably around 400 BCE (Greene et al., 2019).

The onset of the Hellenistic period is marked by a significant increase in Pb contamination (Fig. 6), with traces still evident at the end of antiquity, following the second phase of dredging, and continuing throughout the Medieval to Modern periods. Once again, this change in Pb contamination occurred at a pivotal moment in the history of the Knidia, as the growth of Knidos at Tekir restructured life on the peninsula around the mid-4<sup>th</sup> c. BCE (Bean and Cook, 1952). At Burgaz, this event was accompanied by significant changes, including the abandonment of L1 and likely also L2 and L3 harbor basins, in favor of the newer, larger, and deeper L4 (Greene and Leidwanger, 2019; Greene et al., 2019). However, it is possible the earliest harbor basin L1 continued to host maritime activities on a reduced scale complementary to those of L4, as the older basin was still being dredged at the end of antiquity. Regardless, from the beginning of the Hellenistic period, the port complex and the city underwent a change in function, now focusing on the industrialization of Burgaz (Greene and Leidwanger, 2019). At this time, L4 was home to industrial neighborhoods with workshops and a range of agricultural processing features (Greene et al., 2019). Meanwhile, the occupation of the broader city settlement at Burgaz was discontinued, and certain architectural changes suggest an expansion of spaces for the creation of these workshops, notably dedicated to metalworking (Tuna et al., 2009). Based on (i) the presence of metal workshops in the city, (ii) a water drainage system facilitated by urban planning, steep slopes, and orientation towards the sea (Tuna et al., 2009), (iii) the proximity of L1 to the former urban center, (iv) reduced maritime traffic in L1, and (v) a concentration of new industrial and agricultural activities near L4, we suggest that the Pb palaeo-pollution signal is linked to that of Burgaz. This interpretation is further supported by archaeometric data from the settlement at Burgaz (Kaptan, 2003), where metallurgical artifacts dating to the Classical period show high concentrations of Pb. A certain number of objects, such as U-shaped and spiral lead fragments, lead plate, lead ingot residue, and cylindrical rod, are composed of over 90 % Pb, suggesting deliberate use of lead-based materials. Additionally, trace amounts of Pb (a few hundred ppm) detected in other artifacts indicate broader exposure to Pb in urban and workshop contexts (Kaptan, 2003). These findings reinforce the interpretation of a diffuse urban source of Pb pollution, reflecting spatially and functionally dispersed emissions, consistent with environmental chemistry definitions of diffuse contamination.

#### 5.3.2. Deciphering the natural and anthropogenic Pb isotope signals

Lead has four isotopes,  $^{204}Pb$ ,  $^{206}Pb$ ,  $^{207}Pb$ , and  $^{208}Pb$ , of which only  $^{204}Pb$  is stable while the other three are radiogenic, produced through the decay of  $^{238}U$ ,  $^{235}U$ , and  $^{232}Th$ , respectively. The three distinct radioactive decay chains within the Pb isotope system render Pb isotopes a powerful geochemical tracer (Bird et al., 2010; Bird, 2011). An effective way to differentiate natural and anthropogenic Pb in sediments is to measure the relative abundances of the four Pb isotopes in the residual and leachate fractions of the sediments (Delile et al., 2019). The residual fraction represents the Pb originally incorporated within the mineral crystal lattice at the time of rock formation. This fraction is often described as natural, crustal, detrital, or non-reactive as it reflects the local geogenic Pb background (Bird, 2011). Conversely, the leachate fraction refers to the labile component of Pb that is adsorbed onto sediments after being released from one or more anthropogenic sources. In

principle, Pb from sources of contamination originates from geological regions far removed from the environment where it is eventually deposited as pollution. As a result, the residual and leachate fractions exhibit distinct isotopic signatures. In practice, the leachate component of sediments always includes a contribution from the natural Pb, making the labile fraction a mixture of natural and anthropogenic Pb (Delile et al., 2019).

The results of the Pb isotopic measurements from both the leached (Fig. 7) and residual (Fig. S1) fractions are presented using  $^{204}\text{Pb}$  normalization in the following plots:  $x = {^{206}\text{Pb}}/{^{204}\text{Pb}}$  vs  $y = {^{208}\text{Pb}}/{^{204}\text{Pb}}$ ,  $x = {^{207}\text{Pb}}/{^{204}\text{Pb}}$  vs  $y = {^{208}\text{Pb}}/{^{204}\text{Pb}}$ , and  $x = {^{207}\text{Pb}}/{^{204}\text{Pb}}$  vs  $y = {^{206}\text{Pb}}/{^{204}\text{Pb}}$ . Additionally, the results are shown using the three geochemically informed parameters derived from the measured Pb isotope compositions:  $x = \kappa$  (the tectonic, or geological, "model" age  $T_m$  (Ma) vs  $y = \mu$ ,  $^{232}\text{Th}/^{238}\text{U} \propto \text{Th/U}$ ),  $x = T_m$  vs  $y = \mu$  ( $^{238}\text{U}/^{204}\text{Pb} \propto \text{U/Pb}$ ), and  $x = \kappa$  vs  $y = \mu$ . The use of these parameters has been tested across various disciplinary fields, such as geoarchaeology (e.g., Delile and Keenan-Jones, 2024), archaeometry (e.g., Albarède et al., 2012, 2016, 2020, 2021, 2024a,b; Davis et al., 2025; Blichert-Toft et al., 2022; De Ceuster et al., 2023), and geology (e.g., Bouchet et al., 2014; Blichert-Toft et al., 2016; Milot et al., 2021), due to their ability to (i) overcome the strong correlation of ratios involving  $^{204}\text{Pb}$ , (ii) better isolate sample clusters, (iii) minimize overlaps in ore province signatures, and, finally, (iv) integrate archaeomaterial provenance studies into the regional tectonic history and the dynamic evolution of the continental province (Albarède et al., 2004, 2012). Briefly,  $T_m$  (in million years) reflects tectonic formation ages of the province in question, specifically the most recent U/Pb fractionation event, such as the formation of ores, while  $\kappa$  and  $\mu$  are more likely to reflect deep geological sources. Thus,  $T_m$  identifies geological provinces, while  $\kappa$  and  $\mu$  help distinguish geological segments within them. U/Pb reflects the separation of U and Pb over time within each geological province, representing its metamorphic and hydrothermal evolution (Albarède et al., 2012), while Th/U characterizes lower crustal crust (Bouchet et al., 2014;

Blichert-Toft et al., 2016).

The Pb model ages of the Burgaz harbor sediments clearly distinguish the residual and leachate fractions, with negative (−250 to 0 Ma) and positive (0–150 Ma) ages, respectively (Fig. S1). Negative Pb model ages are indicative of a mantle origin for Pb in areas of high volcanic activity (Albarède et al., 2020; Milot et al., 2021). Geoarchaeological research in the ancient harbor basins of Naples (Delile et al., 2016b) and Rome (Delile et al., 2014; 2017) illustrates particularly well this magmatic component of Pb in volcanic rock-dominated sediments as these harbor deposits exhibit negative  $T_{\text{Mod}}$  (Ma) values for the residual fraction due to the presence of sediments derived from the erosion of the Neapolitan Yellow Tuff from the Phlegraean Fields and modern volcanic deposits from the Alban Hills in Latiun.

The distribution of  $T_{\text{Mod}}$  (Ma) values for the residual fraction in the stratigraphic section shows a progressive increase from ~−250 Ma to ~0 Ma toward the top (Fig. 9A). We tested the assumed linearity of the residual Pb isotopic composition, indicative of a binary mixture of two sedimentary sources, by performing PCA on 204 Pb-normalized data (Baxter and Gale, 1998; Tomczyk and Żabiński, 2023; Albarède et al., 2025). The PCA projection in the three-dimensional component space [ $c_1, c_2, c_3$ ] reveals a dominant variance in  $c_1$  (~90 %), aligning samples along a mixing line between two end-members (upper  $a$  and lower  $b$  end-members in Fig. S2A). Thus, the residual Pb-bearing mineral assemblage likely reflects a time-progressive mixture of two sedimentary sources from the base to the top.  $T_{\text{Mod}}$  (Ma) values correlate strongly ( $r = 0.73$ ) with PCA axis 2 scores, with data points spread according to major chronological periods (Fig. 9B). Given the geological significance of  $T_{\text{Mod}}$  (magmatic vs. crustal) and D2 (marine vs. terrestrial) scores, the pre-harbor unit (HC1, 3.8–2.7 m b.s.l.) corresponds to marine sediments of volcanic origin. From the harbor's foundation (HC2-3, 2.7–0.7 m b.s.l.), sediments show increasing influence of crustal detrital fluxes (Fig. 9). Despite limited knowledge of seafloor sediments along the Datça Peninsula, our findings support Şimşek et al. (2017), who identified Upper Pleistocene to Holocene deposits formed from sedimentary and

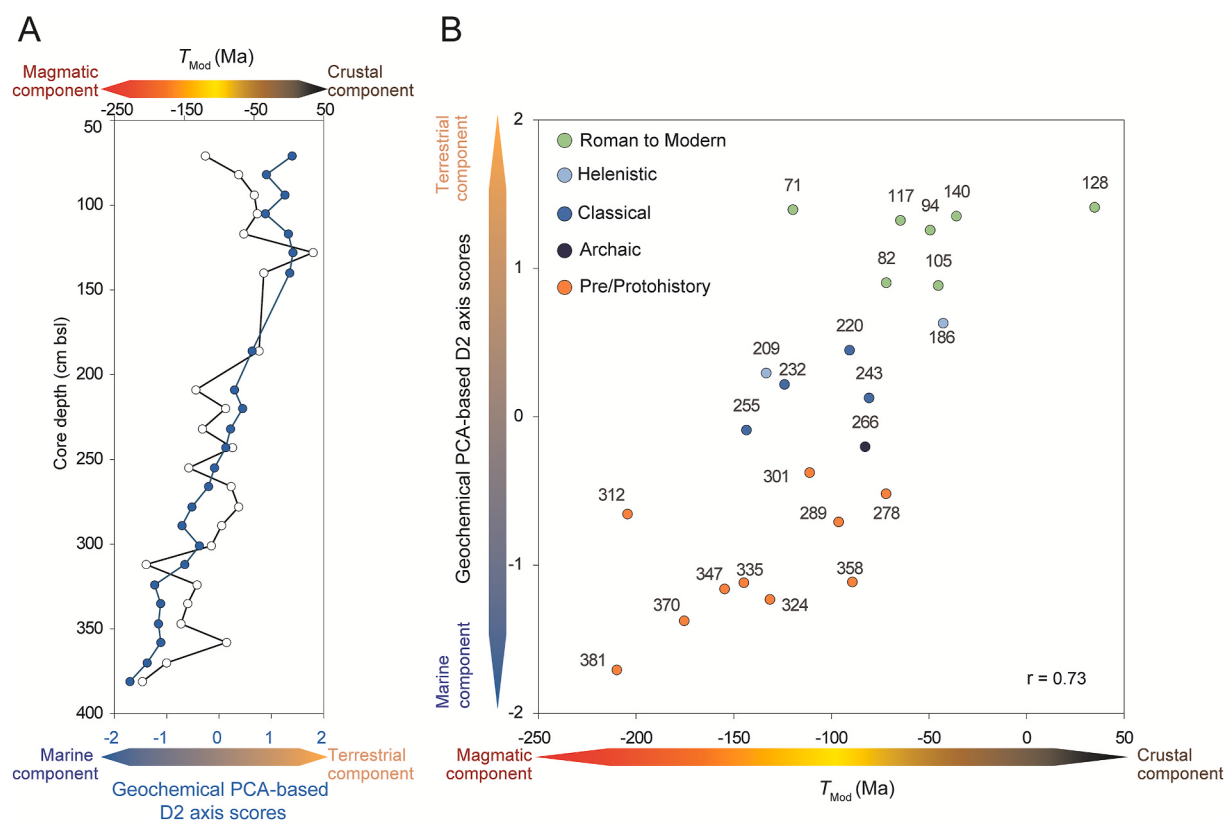


Fig. 9. (A) Stratigraphic variations and (B)  $T_{\text{Mod}}$  (Ma) values for the residual fraction and the geochemical PCA-based D2 axis scores.

magmatic rocks (15000–3000 BP). This context suggests volcanic sources of the seafloor sediments from the Kos-Nisyros-Yali volcanic arc, active during the early Holocene (Koutrouli et al., 2018). Volcanic material likely reached Datça Bay via marine currents and atmospheric pathways (Ercan et al., 2023). Significant late Quaternary eruptions generated ignimbrite and pyroclastic deposits of variable thickness, distributed from Knidos to Burgaz (Allen et al., 1999; Gençalioğlu-Kuçu and Uslular, 2018; Ercan et al., 2023).

For the leached fraction, Pb model ages fall within Alpine values between 0 and 150 Ma (Fig. 7), indicating a common geological basement characteristic of the broader Aegean region (Delile et al., 2014; Westner et al., 2020). This province contrasts with major European basement provinces: Variscan ~350 Ma, Pan-African ~640 Ma, and Svecofennian ~1850 Ma (Blichert-Toft et al., 2016, 2022; Milot et al., 2021). Within this context, parameters  $\mu$  and  $\kappa$  effectively identify coherent sample groups. A U/Pb threshold of ~9.75 distinguishes Pre/Protohistoric sediments from those of the Greek period (Archaic to Hellenistic), while a Th/U threshold of ~3.915 separates Greek from Roman to Modern deposits (Fig. 7). This geochemical complementarity for discriminating lead and silver ore sources has proven effective in the Aegean. Vaxevanopoulos et al. (2022) and Westner et al. (2023) further refined discrimination of eastern Mediterranean mining provinces using  $\mu$  and  $\kappa$  in the Balkans. Crustal segments differ clearly, with higher U/Pb and Th/U values in Macedonia and Thrace versus lower values in the Cyclades, which show a west-to-east gradient. These clusters also appear in the 3D PCA space [c1, c2, c3] of leachates (Fig. S2B), where component c1 (91 %) contrasts Greek period (negative values) with Roman to Modern (positive values) groups, and component c2 (7.6 %) is dominated by the Pre/Protohistoric group. This PCA aligns with Pb enrichment patterns (§5.3.1), as anthropogenic Pb excesses ( $EF_{Pb} > 1.5$ ) from Greek and Roman to Modern groups align with c1, whereas natural background Pb from Pre/Protohistoric deposits aligns with c2 (Fig. S2B). The absence of Pb excess before the Archaic period agrees with archaeological data showing minimal human occupation on the Datça Peninsula prior to 3000 BP. Excavations have revealed no significant Prehistoric settlements or material culture, though deeper volcanic ash-buried layers might hold undiscovered traces.

### 5.3.3. Tracing Pb ore supply sources

This section investigates the potential mining sources of the anthropogenic Pb excesses associated with the Greek and the Roman to Modern groups, offering insights into Burgaz's connections with the broader Mediterranean and their implications for the economic and historical dynamics of these periods. However, it is important to note at the outset that this analysis is limited by the inability to precisely identify the direct sources of contamination of the harbor sediments (see § 5.3.1.). Indeed, depending on whether the primary source is endogenous (e.g., metal workshops, Tuna et al., 2009) or exogenous (e.g., artifacts associated with maritime contexts such as lead hull sheathing or anchor cores, Greene et al., 2019) within the urban center, these potential maritime routes may variously reflect either or both elements of Burgaz's imports from the region or its place as a broader maritime stopover within a wide network that spanned the Aegean and eastern Mediterranean.

Lead isotope signatures are commonly used to determine the provenance of Pb-Ag ore supply sources in the production of Pb-Ag artifacts (e.g., Pernicka et al., 1993; Begemann et al., 2001; Klein et al., 2004; Stos-Gale and Gale, 2009; Albarède et al., 2012; Davis et al., 2025; Heredia et al., 2025). Recent advancements have improved the geolocation of Pb ore sources through a novel algorithm (Albarède et al., 2024a) that statistically measures the distances within the three-dimensional Pb isotope space between artifact compositions and those of ore end-members. These end-members are derived from a new Pb isotope database that accounts for mass-dependent fractionation (Albarède et al., 2024b). Fig. 10 and S3 show the provenance results for all the samples of this study (Fig. S3), using samples K15L and K27L to

represent each of the two major groups (Fig. 10), with their main mining sources summarized in Table 1.

**5.3.3.1. Greek period (Archaic to Hellenistic).** The provenance map of the Greek group highlights the predominance of deposits located in central Greece, the Cyclades, northwestern Sardinia, as well as in Türkiye and Tunisia during this period (Fig. 10 and S3, Table 1). Central Greece, particularly the Laurion mines, was probably the dominant source of metals for the Ancient Greek group, followed by significant contributions from the Cyclades. Western Mediterranean sources, such as Sardinia and Tunisia, appear to have played more peripheral but nonetheless notable roles in the record for Burgaz. The Laurion mines, near Athens, were among the most extensively exploited in the ancient world (e.g. Tylecote, 1992). As early as the 6<sup>th</sup> c. BCE, these mines were closely associated with Athenian Greek coins (Gale et al., 1980; Domergue, 2008; Stos-Gale and Davis, 2020; Albarède et al., 2024a), as well as coins from Greek colonies in Magna Graecia (Birch et al., 2020) and Persian *sigloi* and *Alexanders* (Blichert-Toft et al., 2022). Beyond central Greece, other significant sources of silver have been identified in the coins from this period, particularly from Cycladic origins (e.g., Keos, Seriphos, Kythnos, southern Euboea) and from the Serbomacedonian-Rhodopian Belt (e.g., Rhodope Mountains, Chalkidiki, Pangeon, Thasos, Zletovo) (Birch et al., 2020; Stos-Gale and Davis, 2020; Blichert-Toft et al., 2022; Albarède et al., 2024a,b; Westner et al., 2023). Interestingly, this northern source was not detected among the Pb excess in the first group from Burgaz, a finding that may suggest a less direct connection at the time. In addition to these Aegean sources, other sources common to the Ancient Greek group from Burgaz and to ancient Greek coinage are evident in northwestern Sardinia and Türkiye. Despite the absence of historical and archaeological evidence for silver mining in Sardinia, the incorporation of Sardinian silver into ancient coins from the eastern Mediterranean is sufficiently significant and widespread to warrant the designation of the so-called "old Sardinian mix" (Albarède et al., 2024a). This Sardinian component likely emerged gradually through increasingly frequent trade interactions with the western Mediterranean, established by Phoenician and Greek merchants as early as the 6<sup>th</sup> c. BCE (Parker, 1990). Its origins, however, may extend even further back, as it has also been identified in hoards of hacksilber dating to the Late Bronze and Early Iron Ages from the Levant (Eshel et al., 2019, 2021; Gentelli et al., 2021). A similar contribution from Türkiye is also possible, as several archaeometric studies on ancient Greek silver coins have identified sources in Lydia (Gale et al., 1980; Davis et al., 2025) and, more recently, on the Biga Peninsula in northwestern Anatolia (Birch et al., 2020). Finally, Tunisia has been identified as a potential source of Pb ores, an observation supported by studies tracing metal sources from ancient mints (Birch et al., 2020; Westner et al., 2020; Blichert-Toft et al., 2022; Albarède et al., 2024a). However, this hypothesis remains unverified, as the absence of textual sources and archaeological field studies raises doubts about its validity (Westner et al., 2024). Lead pollution recorded as early as the mid-4<sup>th</sup> c. BCE in sediment cores from the Medjerda delta in Tunisia (Delile et al., 2019) further supports the possibility of mining activity in the Medjerda River basin.

Tracing the Pb ore supply sources for the first group (7<sup>th</sup>-2<sup>nd</sup> c. BCE) at Burgaz shows remarkable consistency with those already well established for Greek silver coinage. This monetization of the Greek economy appears to have been strongly based on the proximity of Pb-Ag ores (Laurion, Euboea) to the Greek city-states, particularly Athens, which facilitated the integration of local mineral resources into a broader regional economic system. In this context, the Cycladic islands, notably Siphnos and Kythnos, likely played a key role in the regional redistribution of metals and in facilitating interactions between mainland Greece and Asia Minor. The Datça Peninsula, located at the intersection of Aegean and Asian maritime routes, would likely have served as a pivotal hub in these networks. Burgaz's strategic location suggests

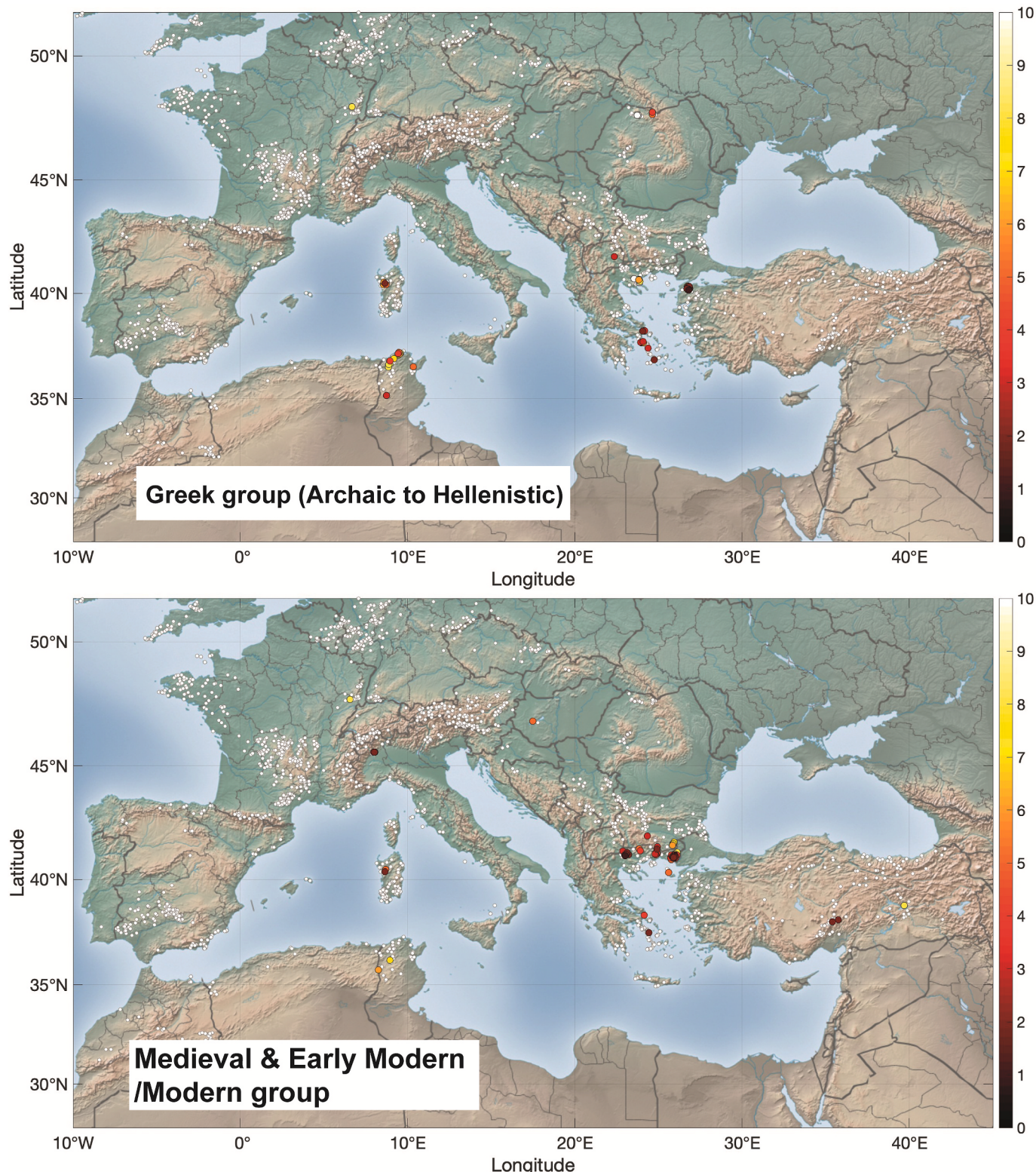


**Fig. 10.** Two representative examples of potential Pb ore supply sources for sediment-bound Pb excesses for the Greek group (Archaic to Hellenistic) (upper map) and the Roman to Modern group (lower map). Data processing is based on the algorithm of Albarède et al. (2024a), which calculates the statistical probability of correspondence between Pb isotope compositions of sediment-bound Pb excesses — sampled at 2.2 m b.s.l. (Greek group) and 0.82 m b.s.l. (Roman to Modern group) — and those from the Lyon Pb isotope database of Pb-Ag ores across Europe and the circum-Mediterranean (white circles). The color scale on the right indicates the reduced distance ( $d$ ) in three-dimensional  $^{204}\text{Pb}$ -normalized Pb isotope ratio space between sediment samples and ores in the database. Darker colors correspond to shorter distances, indicating a closer match between the Pb isotope composition of the sediment sample and the ore plotted on the map. Values exceeding 5.99 fall outside the 95 % confidence level (Albarède et al., 2025). (For interpretation of the references to color in this figure legend, the reader is referred to the Web version of this article.)

**Table 1**

Major hits and other probable provenances of the sediment bound-Pb excesses for the Greek group and the Roman to Modern group.

Data group	Sample	Main supply sources	Additional supply sources
Greek group	K15L	Central Greece (Laurion, Euboea), Aegean islands (Kythnos, Siphnos)	NW Sardinia, NW Turkey, Tunisia
Roman to Early Modern/ Modern group	K27L	Macedonia/Thrace (Serbomacedonian Massif, Rhodopes)	Taurus, NW Sardinia

that it may have acted as both a consumer of Pb-Ag ores and an intermediary hub in redistributing metals within broader routes. Contrary to the traditional model, which attributes the origin of silver in coinage to the southern Balkans and links it to regional commercial networks (Gale et al., 1980; Birch et al., 2020; Stos-Gale and Davis, 2020; Westner et al., 2020; Blichert-Toft et al., 2022; Vaxevanopoulos et al., 2022; Albarède et al., 2024a,b; Westner et al., 2023), the results from Burgaz suggest a stronger connection with the central Mediterranean (Sardinia, Tunisia) despite the fact that the Knidia was very limited in its own establishment of colonies during this wave of Greek expansion outside the Aegean. The absence of Balkan sources in these results suggests a lesser reliance on these regions and a stronger connection with Sardinia and possibly Tunisia, regions well integrated into trans-Mediterranean trade by the 6<sup>th</sup> c. BCE. This pattern indicates that Knidos, more so than other Greek cities, drew heavily on western and central Mediterranean sources, potentially reflecting a strong position within eastern (and broader) Mediterranean trade networks.

**5.3.3.2. Roman to Early Modern/Modern periods.** Excluding isolated hits in northwestern Sardinia, the Taurus region, and ores in the Alps, as well as those from Kythnos and Euboea, the analysis of Pb ore supply sources during the Roman to Modern eras reveals a significant shift toward the ancient provinces of Macedonia and Thrace. The primary identified sources are the Serbomacedonian Massif and the Rhodopes Massif (Fig. 10 and S3, Table 1). Given the substantial historical and archaeological interest in metal production within these regions, recent extensive studies by Vaxevanopoulos et al. (2022) and Westner et al. (2023) have focused on examining their geological features and Pb isotope fingerprints. These studies, combined with historical and archaeological records of mining activities, have significantly enhanced the identification of past mining districts. Cross-referencing our results with these studies suggests that the mining districts of Kilkis/Kroussia, Angiston, and Madan-Thermes were the most likely Pb ore supply sources connected to Burgaz during the Roman to Modern periods.

This transition in Pb ore sources, compared to the Greek period, is also evident in the stratigraphy of Burgaz's harbor at 1.4 m b.s.l., with an age-depth model dating it to 104 BCE (Fig. 7). This shift reflects broader geopolitical and economic transformations at the end of the 2<sup>nd</sup> c. BCE, coinciding with the rise of Roman dominance in the eastern Mediterranean. During this period, the rich ore deposits in the Balkans seem to become central to Roman mining activities following the gradual annexation of Macedonia from 168 BCE (e.g., Nigdelis, 2007; Kay, 2014; Hirt, 2020), after the defeat of King Perseus at the Battle of Pydna. Indeed, the subsequent destruction of Corinth in 146 BCE brought the Greek world under Roman control, integrating its mineral resources into the Empire's economic sphere. The depletion of traditional Greek mining regions (e.g., Strabo IX, I, 24; Patterson, 1972), particularly the Laurion and Cyclades mines, pushed the Romans to exploit the more productive deposits in the Balkans, better suited to meet the growing demand for metals used in coinage, infrastructure, and military equipment. This industrial-scale expansion of mining production under Roman rule in the eastern Mediterranean led to widespread Pb contamination of both Aegean terrestrial and marine ecosystems (Koutsodendris et al., 2025). For Knidos, this historical tipping point

marked a shift from localized economic systems dominated by Greek city-states to a potentially more centralized Roman trade network. Burgaz, once linked to Aegean sources such as central Greece and the Cyclades, became increasingly connected to the Roman-controlled Balkans through maritime routes. This reorientation highlights the adaptability of Burgaz—and probably the Datça Peninsula as a whole—within the broader economic realignments of the eastern Mediterranean, as it transitioned from a regional Greek Aegean-based and eastern Mediterranean network to one of many intermediary nodes in a more expansive Roman system (Leidwanger, 2020).

During the medieval to Modern period, the Pb isotope fingerprints consistently match those of Macedonia and Thrace. This trend aligns with recent findings from atmospheric records in peat bog archives from southeastern Europe, underscoring the enduring influence of central-eastern European medieval metallurgy across diverse environmental and historical contexts (Longman et al., 2024).

## 6. Conclusions

A geoarchaeological approach, aided by geochemical tools, was applied to the earliest harbor basin (L1) at Burgaz to document the environmental dynamics and anthropogenic changes at the site, and to shed new light on the factors that led the community on the Datça Peninsula to shift certain activities and civic focus toward Knidos, at the western end of the peninsula, around the mid-4<sup>th</sup> c. BCE. Our results indicate that the geomorphological configuration of the site was developed during a maximum marine transgression in the early 6<sup>th</sup> mil., shaping the coastal landscape into a very shallow bay in which Burgaz was later founded. The shallow-water conditions at the time of the city's foundation around 700 BCE (Tuna et al., 2009) led to the excavation of the harbor to increase water depth and ensure safe accommodation for ships of a reasonable size and draft (~1.4 m). This initial dredging phase, dated to around 2600 cal BP, triggered a dual imbalance: both in the dynamics of seafloor aggradation and the composition of sediment stocks. During the Middle Holocene, sediment accretion (1.25 mm yr<sup>-1</sup>), primarily composed of volcanic material, was driven by the rate of sea-level rise.

Following the L1 basin's development, this balance was disrupted by the creation of an accommodation space, leading to a sudden increase in sedimentation rates (2.35 mm yr<sup>-1</sup>) during the harbor phase. This dynamic was further intensified by the substantial influx of terrigenous material, driven by Burgaz's pivotal role in the region's agricultural economy, as well as by the construction of moles, which acted as effective sediment traps. The first harbor sediments deposited at the time of the city's foundation recorded an initial, discrete phase of anthropogenic Pb contamination, which later increased during the Classical or very early Hellenistic period. This period coincided with significant urban developments at Burgaz, notably the industrialization of the site and the establishment of metalworking facilities. The associated rise in Pb pollution could thus be the result of diffuse urban emissions, stemming from a combination of artisanal production, domestic activities, and infrastructure-related uses. Archaeometric analyses of metallic artifacts from Burgaz support this interpretation, revealing both high-lead objects and widespread traces of Pb in everyday items, reflecting the pervasive integration of lead into the urban environment. Nonetheless, our research on the mining provenance of these anthropogenic Pb releases revealed that the primary Pb ore supply sources were located in central Greece and the Cyclades from the Archaic to the Hellenistic period. Burgaz, situated at the intersection of Aegean and eastern Mediterranean maritime routes, likely served as a hub within these networks. If the shift in civic and economic emphasis toward the end of the peninsula from the 4<sup>th</sup> c. BCE is related to changes in the broader networks to which the peninsula was connected, this is certainly not reflected in any shifts in Pb origins, as the mining supply sources remained stable until the end of the 2<sup>nd</sup> c. BCE. However, the rise of Roman power in the eastern Mediterranean a few centuries after this

shift seems, by contrast, to have significantly altered the map of primary lead ore supply sources, which reoriented toward the northern Aegean. The Pb isotopic compositions of harbor sediments point to the mining districts of the Serbomacedonian Massif and the Rhodopes Massif. This reorientation highlights Burgaz's adaptability within the broader economic realignments of the eastern Mediterranean, as it transitioned from being part of a regional network to a node within the more expansive Roman trade system, a system that flourished all the more here in Late Antiquity (Leidwanger, 2020), and which later extended into the medieval period.

It should be noted that maintenance of the first harbor basin of Burgaz appears to have been sustained until the end of antiquity, with a second phase of dredging identified during this period. This suggests a deliberate effort to preserve a multi-scale harbor system, characterized by a network of small and interlinked basins both at Burgaz (from L1 to L4) and more broadly across the peninsula. Together with the dual basins at the port of Knidos, these formed a complex harbor system that integrated and mobilized regional agricultural and other products. Through this system, the booming agriculture of the Knidia reached broader markets, which in turn brought the products of a growing regional and then imperial economy to the larger and smaller communities across the Datça Peninsula (Greene and Leidwanger, 2019, 2022; Leidwanger, 2019).

#### CRediT authorship contribution statement

**H. Delile:** Conceptualization, Methodology, Formal analysis, Writing – original draft, Visualization, Laboratory Formal analysis, Data curation, Formal analysis, Validation, Funding acquisition. **J. Leidwanger:** Investigation, Resources, Funding acquisition, Supervision, Project administration, Writing – review & editing. **J.-P. Goiran:** Investigation, Resources, Writing – review & editing. **J. Blichert-Toft:** Resources, Validation, Writing – review & editing. **F. Stock:** Investigation, Formal analysis, Writing – review & editing. **G. Brocard:** Investigation. **L. Radloff:** Investigation, Supervision, Project administration, Writing – review & editing. **E.S. Greene:** Investigation, Resources, Funding acquisition, Supervision, Project administration, Writing – review & editing. **N. Tuna:** Investigation, Resources, Funding acquisition, Project administration, Writing – review & editing.

#### Declaration of competing interest

The authors declare that they have no known competing financial interests or personal relationships that could have appeared to influence the work reported in this paper.

#### Acknowledgements

Thanks are due to the Turkish Ministry of Culture and Tourism for permission to conduct research at Burgaz, and to the organizations that provided financial and logistical support for the harbor research: the Social Sciences and Humanities Research Council of Canada, Loeb Classical Library Foundation, Honor Frost Foundation, Canada Foundation for Innovation, Stanford University's Department of Classics and its Archaeology Center, Brock University, Middle East Technical University, Institute of Nautical Archaeology, and Maison de l'Orient et de la Méditerranée Jean Pouilloux (internal call for projects MOM 2016). We further acknowledge the ARTEMIS-SHS program and radiocarbon laboratory of Lyon for carrying out the radiocarbon dating. This work was conducted using analytical support from the OMEAA technology platform (UMR 5600 and UMR 5133 CNRS) based at the University Lumière Lyon 2.

#### Appendix A. Supplementary data

Supplementary data to this article can be found online at <https://doi.org/10.1016/j.quascirev.2025.109526>.

<https://doi.org/10.1016/j.quascirev.2025.109526>.

#### Data availability

All data and/or code is contained within the submission.

#### References

- Albarède, F., 1995. Introduction to Geochemical Modeling. Cambridge University Press, Cambridge. <https://doi.org/10.1017/CBO9780511622960>.
- Albarède, F., Telouk, P., Blichert-Toft, J., Boyet, M., Agranier, A., Nelson, B., 2004. Precise and accurate isotopic measurements using multiple-collector ICPMS1. *Geochim. Cosmochim. Acta* 68, 2725–2744. <https://doi.org/10.1016/j.gca.2003.11.024>.
- Albarède, F., Davis, G., Gitler, H., Blichert-Toft, J., Gentelli, L., 2025. Levantine Hacksilber and the flow of silver in early Mediterranean commerce. *Archaeometry* n/a. <https://doi.org/10.1111/arcm.70006>.
- Albarède, F., Desaulny, A.-M., Blichert-Toft, J., 2012. A geological perspective on the use of Pb isotopes in archaeometry. *Archaeometry* 54, 853–867. <https://doi.org/10.1111/j.1475-4754.2011.00653.x>.
- Albarède, F., Blichert-Toft, J., Rivoal, M., Telouk, P., 2016. A glimpse into the Roman finances of the second Punic War through silver isotopes. *Geochemical Perspectives Letters* 127–137. <https://doi.org/10.7185/geochemlet.1613>.
- Albarède, F., Blichert-Toft, J., Gentelli, L., Milo, J., Vaxevanopoulos, M., Klein, S., Westner, K., Birch, T., Davis, G., de Callatay, F., 2020. A miner's perspective on Pb isotope provenances in the Western and Central mediterranean. *J. Archaeol. Sci.* 121, 105194. <https://doi.org/10.1016/j.jas.2020.105194>.
- Albarède, F., Blichert-Toft, J., de Callatay, F., Davis, G., Debernardi, P., Gentelli, L., Gitler, H., Kemmers, F., Klein, S., Malod-Dognin, C., Milo, J., Telouk, P., Vaxevanopoulos, M., Westner, K., 2021. From commodity to money: the rise of silver coinage around the Ancient mediterranean (sixth–first centuries bce). *Archaeometry* 63, 142–155. <https://doi.org/10.1111/arcm.12615>.
- Albarède, F., Blichert-Toft, J., Gentelli, L., Gitler, H., Pinto, M., Telouk, P., 2024a. A new algorithm for using Pb isotopes to determine the provenance of bullion in ancient Greek coinage. *J. Archaeol. Sci.* 163, 105919. <https://doi.org/10.1016/j.jas.2023.105919>.
- Albarède, F., Davis, G., Gentelli, L., Blichert-Toft, J., Gitler, H., Pinto, M., Telouk, P., 2024b. Bullion mixtures in silver coinage from ancient Greece and Egypt. *J. Archaeol. Sci.* 162, 105918. <https://doi.org/10.1016/j.jas.2023.105918>.
- Alcock, S.E., 1993. *Gracia Capta: the Landscapes of Roman Greece*. Cambridge University Press, Cambridge, Royaume-Uni de Grande-Bretagne et d'Irlande du Nord.
- Allen, S.R., Stadlbauer, E., Keller, J., 1999. Stratigraphy of the Kos Plateau Tuff: product of a major Quaternary explosive rhyolitic eruption in the eastern Aegean, Greece. *Int. J. Earth Sci.* 88, 132–156. <https://doi.org/10.1007/s005310050251>.
- Altunel, E., Stenwart, I., Piccardi, L., Barka, A.A., 2003. Earthquake faulting at ancient Cnidus, SW Türkiye. *Turk. J. Earth Sci.* 12, 137–151.
- Anzidei, M., Antonioli, F., Benini, A., Lambeck, K., Sivan, D., Serpelloni, E., Stocchi, P., 2011. Sea level change and vertical land movements since the last two millennia along the coasts of Southwestern Türkiye and Israel. *Quaternary International, Tectonic Contribution to Relative Sea Level Change* 232, 13–20. <https://doi.org/10.1016/j.quaint.2010.05.005>.
- Auriemma, R., Solinas, E., 2009. Archaeological remains as sea level change markers: a review. *Quaternary International, Continental Shelves: Sea Levels and Environments* 206, 134–146. <https://doi.org/10.1016/j.quaint.2008.11.012>.
- Baxter, M.J., Gale, N.H., 1998. Testing for multivariate normality via univariate tests: a case study using lead isotope ratio data. *J. Appl. Stat.* 25, 671–683. <https://doi.org/10.1080/02664769822891>.
- Bean, G.E., Cook, J.M., 1952. The Cnidia. *Annu. Br. Sch. A. T. Athens* 47, 171–212. <https://doi.org/10.1017/S0068245400012338>.
- Begemann, F., Schmitt-Strecker, S., Pernicka, E., Lo Schiavo, F., 2001. Chemical composition and lead isotopy of copper and bronze from nuragic sardinia. *Eur. J. Archaeol.* 4, 43–85.
- Berges, D., 1994. Alt-Knidos und Neu-Knidos. *Istanbuler Mitteilungen* 44, 5–16.
- Bertrand, S., Tjallingii, R., Kylander, M.E., Wilhelm, B., Roberts, S.J., Arnaud, F., Brown, E., Bindler, R., 2024. Inorganic geochemistry of lake sediments: a review of analytical techniques and guidelines for data interpretation. *Earth Sci. Rev.* 249, 104639. <https://doi.org/10.1016/j.earscirev.2023.104639>.
- Bietak, M., 1981. *Avaris and Piramesse: Archaeological Exploration in the Eastern Nile Delta*. Oxford University Press, Oxford, Royaume-Uni de Grande-Bretagne et d'Irlande du Nord.
- Birch, T., Westner, K.J., Kemmers, F., Klein, S., Höfer, H.E., Seitz, H.-M., 2020. Retracing Magna Graecia's silver: coupling lead isotopes with a multi-standard trace element procedure. *Archaeometry* 62, 81–108. <https://doi.org/10.1111/arcm.12499>.
- Bird, G., 2011. Provenancing anthropogenic Pb within the fluvial environment: developments and challenges in the use of Pb isotopes. *Environ. Int.* 37, 802–819. <https://doi.org/10.1016/j.envint.2011.02.007>.
- Bird, G., Brewer, P.A., Macklin, M.G., Nikolova, M., Kotsev, T., Mollov, M., Swain, C., 2010. Quantifying sediment-associated metal dispersals using Pb isotopes: application of binary and multivariate mixing models at the catchment-scale. *Environ. Pollut.* 158, 2158–2169. <https://doi.org/10.1016/j.envpol.2010.02.020>.
- Blaauw, M., 2010. Methods and code for 'classical' age-modelling of radiocarbon sequences. *Quat. Geochronol.* 5, 512–518. <https://doi.org/10.1016/j.quageo.2010.01.002>.

- Blichert-Toft, J., Delile, H., Lee, C.-T., Stos-Gale, Z., Billström, K., Andersen, T., Hannu, H., Albarède, F., 2016. Large-scale tectonic cycles in Europe revealed by distinct Pb isotope provinces. *G-cubed* 17, 3854–3864.
- Blichert-Toft, J., de Callataÿ, F., Télouk, P., Albarède, F., 2022. Origin and fate of the greatest accumulation of silver in ancient history. *Archaeol. Anthropol. Sci.* 14, 64. <https://doi.org/10.1007/s12520-022-01537-y>.
- Blott, S.J., Pye, K., 2001. GRADISTAT: a grain size distribution and statistics package for the analysis of unconsolidated sediments. *Earth Surf. Process. Landf.* 26, 1237–1248. <https://doi.org/10.1002/esp.261>.
- Blümel, W., 1992. Die Inschriften von Knidos I [IK 41]. Habelt, Bonn.
- Boetto, G., 2010. Le port vu de la mer : l'apport de l'archéologie navale à l'étude des ports antiques. In: Keay, S., Boetto, G. (Eds.), *Portus, Ostia and the Ports of the Roman Mediterranean. Contributions from Archaeology and History, Proceedings of the 17th International Congress of Classical Archaeology, Rome 2008*, Rome, pp. 112–128.
- Bouchet, R.A., Blichert-Toft, J., Reid, M.R., Levander, A., Albarède, F., 2014. Similarities between the Th/U map of the western US crystalline basement and the seismic properties of the underlying lithosphere. *Earth Planet Sci. Lett.* 391, 243–254. <https://doi.org/10.1016/j.epsl.2014.02.004>.
- Bouton, S.J., Stewart, I.S., 2015. Holocene coastal notches in the Mediterranean region: indicators of paleoseismic clustering? *Geomorphology, Geomorphology of Active Faulting and seismic hazard assessment: New tools and future challenges* 237, 29–37. <https://doi.org/10.1016/j.geomorph.2013.11.012>.
- Bresson, A., 1999. Cnide à l'époque classique: la cité et ses villes. <https://doi.org/10.3406/reia.1999.4760>.
- Bruins, H.J., MacGillivray, J.A., Synolakis, C.E., Benjamini, C., Keller, J., Kisch, H.J., Klügel, A., van der Plicht, J., 2008. Gearchaeological tsunami deposits at Palaiastro (Crete) and the Late Minoan IA eruption of Santorini. *J. Archaeol. Sci.* 35, 191–212. <https://doi.org/10.1016/j.jas.2007.08.017>.
- Büyüközer, A., 2012. *Knidos Limanları*. Phd Dissertation. Selçuk University.
- Büyüközer, A., 2013. Some thoughts on the military harbour of Knidos. In: Morozova, Y., Öñiz, H. (Eds.), *SOMA 2010: Proceedings of 14th Symposium on Mediterranean Archaeology*, Taras Sevchenko National University of Kiev, Kiev, Ukraine, April 2010. BAR Publishing, Oxford, pp. 11–16. <https://doi.org/10.30861/9781407311760>.
- Carsana, V., Febrero, S., Giampaola, D., Guastaferro, C., Irollo, G., Ruello, M.R., 2009. Evoluzione del paesaggio costiero tra Panoponee Neapolis. *Méditerranée* 14–22. <https://doi.org/10.4000/mediterranee.2943>.
- Ceuster, S.D., Machaira, D., Degryse, P., 2023. Lead isotope analysis for provenancing ancient materials: a comparison of approaches. *RSC Adv.* 13, 19595–19606. <https://doi.org/10.1039/D3RA02763E>.
- Chabrol, A., Delile, H., Baron, S., Bouras, C., Athanasopoulos, P., Lovén, B., 2023. Harbour geoarchaeology of Lechaion (corinth area, Greece) sheds new light on economics during the late Bronze Age/Early Iron Age transition. *Mar. Geol.* 465, 107167. <https://doi.org/10.1016/j.margeo.2023.107167>.
- Chapkanski, S., Goiran, J.-P., Rosa, C., Kay, S., Graauw, A. de, Gallet, X., D’Ottavio, D., Keay, S., 2021. Infrared spectroscopic investigations of the Northern Mole of Portus, the Ancient harbour of Rome. Insights for stratigraphy and provenance of raw materials for construction. *Mediterranean Archaeology and Archaeometry* 21, 227.
- Cooke, C.A., Abbott, M.B., Wolfe, A.P., Kittleson, J.L., 2007. A millennium of metallurgy recorded by lake sediments from Morococha, Peruvian Andes. *Environ. Sci. Technol.* 41, 3469–3474. <https://doi.org/10.1021/es062930+>.
- Davis, G., Blichert-Toft, J., Gentelli, L., Gore, D.B., Sheedy, K.A., Albarède, F., 2025. Identifying silver ore sources for the earliest coins of Athens. *Archaeol. Anthropol. Sci.* 17, 45. <https://doi.org/10.1007/s12520-024-02120-3>.
- Delile, H., 2014. Signatures des paléo-pollution et des paléoenvironnements dans les archives sédimentaires des ports antiques de Rome et d’Éphèse (Doctorat de géographie/géochronologie). Université Lumière Lyon 2. Lyon.
- Delile, H., Keenan-Jones, D., 2024. Production-consumption-release of trace metal elements, the urban proxies of the palaeo-anthropocene. In: Salomon, F., Borderie, Q. (Eds.), *Urban Geoarchaeology*, pp. 133–152. Paris.
- Delile, H., Salomon, F., 2020. Palaeotsunami deposits at the Tiber River mouth (Ostia Antica, Italy): do they really exist? *Earth Sci. Rev.* 208, 103268. <https://doi.org/10.1016/j.earscirev.2020.103268>.
- Delile, H., Mazzini, I., Blichert-Toft, J., Goiran, J.-P., Arnaud-Godet, F., Salomon, F., Albarède, F., 2014a. Geochemical investigation of a sediment core from the Trajan basin at Portus, the harbor of ancient Rome. *Quat. Sci. Rev.* 87, 34–45.
- Delile, H., Blichert-Toft, J., Goiran, J.-P., Keay, S., Albarède, F., 2014b. Lead in ancient Rome’s city waters. *Proc. Natl. Acad. Sci. USA* 111, 6594–6599. <https://doi.org/10.1073/pnas.140097111>.
- Delile, H., Blichert-Toft, J., Goiran, J.-P., Stock, F., Arnaud-Godet, F., Bravard, J.-P., Brückner, H., Albarède, F., 2015. Demise of a harbor: a geochemical chronicle from Ephesus. *J. Archaeol. Sci.* 53, 202–213. <https://doi.org/10.1016/j.jas.2014.10.002>.
- Delile, H., Goiran, J.-P., Blichert-Toft, J., Arnaud-Godet, F., Romano, P., Bravard, J.-P., 2016a. A geochemical and sedimentological perspective of the life cycle of Neapolis harbor (Naples, southern Italy). *Quat. Sci. Rev.* 150, 84–97. <https://doi.org/10.1016/j.quascirev.2016.08.026>.
- Delile, H., Keenan-Jones, D., Blichert-Toft, J., Goiran, J.-P., Arnaud-Godet, F., Romano, P., Albarède, F., 2016b. A lead isotope perspective on urban development in ancient Naples. *Proc. Natl. Acad. Sci. USA* 113, 6148–6153. <https://doi.org/10.1073/pnas.1600893113>.
- Delile, H., Keenan-Jones, D., Blichert-Toft, J., Goiran, J.-P., Arnaud-Godet, F., Albarède, F., 2017. Rome’s urban history inferred from Pb-contaminated waters trapped in its ancient harbor basins. *Proc. Natl. Acad. Sci.* 114, 10059–10064.
- Delile, H., Goiran, J.P., Blichert-Toft, J., 2018. The contribution of geochemistry to ancient harbor geoarchaeology: the example of Ostia Antica. *Quat. Sci. Rev.* 193, 170–187. <https://doi.org/10.1016/j.quascirev.2018.06.019>.
- Delile, H., Pleuger, E., Blichert-Toft, J., Goiran, J.-P., Fagel, N., Gadhoum, A., Abichou, A., Jerbania, I.B., Fentress, E., Wilson, A.I., 2019. Economic resilience of Carthage during the Punic Wars: insights from sediments of the Medjerda delta around Utica (Tunisia). *Proc. Natl. Acad. Sci. USA* 116, 9764–9769. <https://doi.org/10.1073/pnas.1821015116>.
- Demand, N., 1989. Did Knidos really move? The literary and epigraphical evidence. *Class. Antiq.* 8 (2), 224–237.
- Demand, N., 1990. *Urban Relocation in Archaic and Classical Greece*. University of Oklahoma Press, Norman.
- Dirik, K., 2007. Tectonic characteristics and seismicity of the Resadiye (Datça) peninsula and surrounding area, Southwest Anatolia. *Geol. Bull. Turk.* 50, 130–149.
- Doksanaltı, E.M., 2007. Knidos-Kap Krio yerleşim alanı. İDOL: Arkeologlar Derneği Dergisi 9 (33), 2–11.
- Doksanaltı, E.M., Sevmen, D., Karaoglan, İ., Özgan, C., Aslan, E., 2016. Knidos kazı ve araştırmaları: 2014. Kazı Sonuçları Toplantısı 37 (3), 57–81.
- Doksanaltı, E.M., Karaoglan, İ., Tozluca, D.O., 2018. Knidos: denizlerin buluştuğu kent. Bilgin Kültür Sanat Yayınları, Ankara.
- Domergue, C., 2008. Les mines antiques : la production des métaux aux époques grecque et romaine. *Antiqua* (Paris). Picard, Paris, France.
- Eisele, J., Abouchami, W., Galer, S.J.G., Hofmann, A.W., 2003. The 320 kyr Pb isotope evolution of Mauna Kea lavas recorded in the HSDP-2 drill core. *G-cubed* 4, 1–32. <https://doi.org/10.1016/j.gca.2002902002GC000339>.
- Elmaleh, A., Galy, A., Allard, T., Dairon, R., Day, J.A., Michel, F., Marriner, N., Morhange, C., Couffignal, F., 2012. Anthropogenic accumulation of metals and metalloids in carbonate-rich sediments: insights from the ancient harbor setting of Tyre (Lebanon). *Geochem. Cosmochim. Acta* 82, 23–38. <https://doi.org/10.1016/j.gca.2011.04.032>.
- Ercan, T., Günay, E., Baş, H., Can, B., 2023. Petrology and interpretation of the origin of Quaternary volcanics in the Datça Peninsula. *Bulletin of the Mineral Research and Exploration* 1981.
- Eshel, T., Erel, Y., Yahalom-Mack, N., Tirosh, O., Gilboa, A., 2019. Lead isotopes in silver reveal earliest Phoenician quest for metals in the west Mediterranean. *Proc. Natl. Acad. Sci. USA* 116, 6007–6012. <https://doi.org/10.1073/pnas.1817951116>.
- Eshel, T., Gilboa, A., Yahalom-Mack, N., Tirosh, O., Erel, Y., 2021. Debasing of silver throughout the late Bronze – Iron Age transition in the Southern Levant: analytical and cultural implications. *J. Archaeol. Sci.* 125, 105268. <https://doi.org/10.1016/j.jas.2020.105268>.
- Evans, R.J., 2014. The capture of Sybaris (510 BC) and the siege of Mantinea: history repeated? *Acta Class.* 57, 225–232.
- Flemming, N.C., Czartoryska, N.M.G., Hunter, P.M., 1971. Archaeological evidence for eustatic and tectonic components of relative sea-level changes in the South Aegean. In: Blackman, D.J. (Ed.), *Marine Archaeology*. Butterworths, London, pp. 1–63.
- Gale, N.H., Gentner, W., Wagner, G.A., 1980. Mineralogical and geographical sources of archaic Greek coinage. In: Metcalf, D.A., Oddy, W.A. (Eds.), *Metallurgy in Numismatics*, the Royal Numismatic Society. Royal Numismatic Society, London, pp. 3–49.
- Gençalioglu-Kuşcu, G., Uslular, G., 2018. Geochemical characterization of mid-distal Nisyros tephra on Datça peninsula (southwestern Anatolia). *J. Volcanol. Geoth. Res.* 354, 13–28. <https://doi.org/10.1016/j.jvolgeores.2017.12.011>.
- Gentelli, L., Blichert-Toft, J., Davis, G., Gitler, H., Albarède, F., 2021. Metal provenance of Iron Age Hacksilber hoards in the southern Levant. *J. Archaeol. Sci.* 134, 105472. <https://doi.org/10.1016/j.jas.2021.105472>.
- Giaime, M., Marriner, N., Morhange, C., 2019. Evolution of ancient harbours in deltaic contexts: a geoarchaeological typology. *Earth Sci. Rev.* 191, 141–167. <https://doi.org/10.1016/j.earscirev.2019.01.022>.
- Gogou, M., Mavroulis, S., Evelpidou, N., Lekkas, E., 2022. Earthquakes and Tsunamis: Natural Hazards over the Aegean Archipelago. Springer, Berlin, Heidelberg, pp. 1–38. [https://doi.org/10.1007/978\\_2022\\_941](https://doi.org/10.1007/978_2022_941).
- Goiran, J.-P., 2001. Recherches géomorphologiques dans la région littorale d’Alexandrie en Egypte. Université De Provence (Aix-Marseille).
- Goiran, J.-P., Morhange, C., 2003. Géoarchéologie des ports antiques en Méditerranée : problématiques et études de cas. *Topoi* 647–669.
- Goiran, J.-P., Tronchère, H., Salomon, F., Carbonel, P., Djerbi, H., Ognard, C., 2010. Palaeoenvironmental reconstruction of the ancient harbors of Rome: Claudius and Trajan’s marine harbors on the Tiber delta. *Quaternary International, Landscape Evolution and Gearchaeology* 216, 3–13. <https://doi.org/10.1016/j.quaint.2009.10.030>.
- Goiran, J.-P., Pavlopoulos, K.P., Fouache, E., Triantaphyllou, M., Etienne, R., 2011a. Piraeus, the ancient island of Athens: evidence from Holocene sediments and historical archives. *Geology* 39 (1), 531–534. <https://doi.org/10.1130/G31818>.
- Goiran, J.-P., Salomon, F., Tronchère, H., Djerbi, H., Carbonel, P., Ognard, C., Oberlin, C., 2011b. Géoarchéologie des ports de Claude et de Trajan, Portus, delta du Tibre. *Mélanges de l’École française de Rome - Antiquité*, pp. 157–236. <https://doi.org/10.4000/mefra.491>.
- Goiran, J.-P., Salomon, F., Mazzini, I., Bravard, J.-P., Pleuger, E., Vittori, C., Boetto, G., Christiansen, J., Arnaud, P., Pellegrino, A., Pepe, C., Sadori, L., 2014. Geochronology confirms location of the ancient harbour basin of Ostia (Italy). *J. Archaeol. Sci.* 41, 389–398. <https://doi.org/10.1016/j.jas.2013.08.019>.
- Goiran, J.-P., Chan, W.M., Benech, C., Vitale, Q., Riddick, N., Delile, H., Salomon, F., Chapkanski, S., Oberlin, C., Brocard, G., Lisé-Pronost, A., Vittori, C., 2022. Developments in geoarchaeological research, methodologies and applications in Harbour maritime archaeology. In: Preiser-Kapeller, J., Kolas, T., Daim, F. (Eds.), *Seasides of Byzantium: Harbours and Anchorages of a Mediterranean Empire*,

- Byzanz zwischen Orient und Okzident. Propylaeum, Heidelberg, pp. 109–129. <https://doi.org/10.11588/propylaeum.910>.
- Graham, G., 1997. Tanis. In: Meyers, E. (Ed.), *Oxford Encyclopedia of the Ancient Near East*, pp. 348–350. New York.
- Greene, E.S., Leidwanger, J., 2019. Knidian “Anyports”: a model of coastal adaptation and socioeconomic connectivity from southwest Turkey. *Mediterr. Hist. Rev.* 34, 9–25. <https://doi.org/10.1080/09518967.2018.1535396>.
- Greene, E.S., Leidwanger, J., 2022. Wandering ports on the Datça Peninsula: exploring regional mobility in a maritime landscape. In: Daniels, M. (Ed.), *Homo Migrans: Modeling Mobility and Migration in Human History*. SUNY Press, Albany, pp. 269–290. <https://doi.org/10.2307/jj.18254836.17>.
- Greene, E.S., Leidwanger, J., Tuna, N., 2019. Archaeological Investigations in the Harbours of Burgaz, Turkey: 2011–2015 field seasons. *Int. J. Naut. Archaeol.* 48, 103–122. <https://doi.org/10.1111/1095-9270.12334>.
- Guédron, S., Tolu, J., Delaere, C., Sabatier, P., Barre, J., Heredia, C., Brisset, E., Campillo, S., Bindler, R., Fritz, S.C., Baker, P.A., Amouroux, D., 2021. Reconstructing two millennia of copper and silver metallurgy in the Lake Titicaca region (Bolivia/Peru) using trace metals and lead isotopic composition. *Anthropocene* 34, 100288. <https://doi.org/10.1016/j.jancene.2021.100288>.
- Guidoboni, E., Comastri, A., Traina, G., Istituto nazionale di geofisica, 1994. Catalogue of Ancient Earthquakes in the Mediterranean Area up to the 10th C. Istituto nazionale di geofisica, Rome, Italie.
- Hall, G.F., Hill, D.F., Horton, B.P., Engelhart, S.E., Peltier, W.R., 2013. A high-resolution study of tides in the Delaware Bay: past conditions and future scenarios. *Geophys. Res. Lett.* 40, 338–342. <https://doi.org/10.1029/2012GL054675>.
- Heredia, C., Guédron, S., Gourlan, A.T., Helly, B., Delile, H., Calzolari, L., Campillo, S., Santenac, S., Audin, L., Telouk, P., Albareda, F., 2025. Provenance of lead ores used for water pipes production in the ancient Roman Gaul (Vienne, France). *Quat. Sci. Rev.* 353, 109227. <https://doi.org/10.1016/j.quascirev.2025.109227>.
- Hirt, A., 2020. Gold and silver mining in the Roman Empire. In: Butcher, K. (Ed.), *Debasement: Manipulation of Coin Standards in Pre-modern Monetary Systems*. Oxbow books, Oxford Philadelphia, pp. 111–124.
- Hoffmeier, J.K., Rendsburg, G.A., 2022. Pithom and Rameses (Exodus 1:11): historical, archaeological, and linguistic issues (part I). *Journal of Ancient Egyptian Interconnections* 33, 1–19.
- Holdridge, G., Kristiansen, S.M., Barfod, G.H., Kinnauld, T.C., Lichtenberger, A., Olsen, J., Philippißen, B., Raja, R., Simpson, I., 2021. A Roman provincial city and its contamination legacy from artisanal and daily-life activities. *PLoS One* 16, e0251923. <https://doi.org/10.1371/journal.pone.0251923>.
- İşcan, Y., Tur, H., Gökaşan, E., 2013. Morphologic and seismic features of the Gulf of Gökova, SW Anatolia: evidence of strike-slip faulting with compression in the Aegean extensional regime. *Geo-Mar. Lett.* 33, 31–48. <https://doi.org/10.1007/s00367-012-0307-x>.
- Kaptan, E., 2003. Burgaz 2000 yılı kazısına ait maden cırıfları ile işlenmiş metal buluntular. MTA Genel Müdürlüğü Tabiat Tarihi Müzesi Rapor 33, 18.
- Kay, P., 2014. *Rome's Economic Revolution*. Oxford University Press, Oxford. Royaume-Uni de Grande-Bretagne et d'Irlande du Nord.
- Kayan, İ., 1988. Late Holocene sea-level changes on the western Anatolian coast. *Palaeogeography, Palaeoclimatology, Palaeoecology, Quaternary Coastal Changes* 68, 205–218. [https://doi.org/10.1016/0031-0182\(88\)90040-5](https://doi.org/10.1016/0031-0182(88)90040-5).
- Keay, S., 2012. Portus. In: *The Encyclopedia of Ancient History*. Blackwell Publishing Ltd.
- Keay, S., Millett, M., Paroli, L., 2005. Portus: an Archaeological Survey of the Portus of Imperial Rome. *Archaeological Monographs of the British School at Rome*, 15. British School at Rome, London.
- Kızıldağ, N., Özdas, A.H., Uluğ, A., 2012. Late Pleistocene and Holocene Sea level changes in the Hisarönü Gulf, Southeast Aegean Sea. *Geoarchaeology* 27, 220–236. <https://doi.org/10.1002/gea.21407>.
- Klein, S., Lahaye, Y., Brey, G.P., Von Kaelen, H.-M., 2004. The early Roman imperial AES coinage II: tracing the copper sources by analysis of lead and copper isotopes—copper coins of Augustus and Tiberius. *Archaeometry* 46, 469–480. <https://doi.org/10.1111/j.1475-4754.2004.00168.x>.
- Koparal, E., Tuna, N., İplikçi, A.E., 2014. Hellenistic wine press in Burgaz/Old Knidos. *METU Journal of the Faculty of Architecture* 31 (2), 93–107.
- Koutrouli, A., Anastasakis, G., Kontakiotis, G., Ballengee, S., Kuehn, S., Pe-Piper, G., Piper, D.J.W., 2018. The early to mid-Holocene marine tephrrostratigraphic record in the Nisyros-Yali-Kos volcanic center, SE Aegean Sea. *J. Volcanol. Geoth. Res.* 366, 96–111. <https://doi.org/10.1016/j.jvolgeores.2018.10.004>.
- Koutsodendris, A., Maran, J., Kotthoff, U., Lippold, J., Knipping, M., Friedrich, O., Gerdes, A., Kaboth-Bahr, S., Bahr, A., Schulz, H., Sakellariou, D., Pross, J., 2025. Societal changes in ancient Greece impacted terrestrial and marine environments. *Commun. Earth Environ.* 6, 1–10. <https://doi.org/10.1038/s43247-024-01921-7>.
- Kraft, J.C., Kayan, I., Brückner, H., Rapp, G., 2000. A geological analysis of ancient landscapes and the harbors of Ephesus and the Artemision in Anatolia. In: *Jahreshefte des Österreichischen Archäologischen Institutes in Wien*, pp. 175–233.
- Lambeck, K., Bard, E., 2000. Sea-level change along the French Mediterranean coast for the past 30 000 years. *Earth Planet Sci. Lett.* 175, 203–222. [https://doi.org/10.1016/S0012-821X\(99\)00289-7](https://doi.org/10.1016/S0012-821X(99)00289-7).
- Lambeck, K., Purcell, A., 2005. Sea-level change in the Mediterranean Sea since the LGM: model predictions for tectonically stable areas. *Quaternary Science Reviews*, *Quaternary coastal morphology and sea-level changes* 24, 1969–1988. <https://doi.org/10.1016/j.quascirev.2004.06.025>.
- Lambeck, K., Rouby, H., Purcell, A., Sun, Y., Cambridge, M., 2014. Sea level and global ice volumes from the Last Glacial Maximum to the Holocene. *Proc. Natl. Acad. Sci. U. S. A.* 111, 15296–15303. <https://doi.org/10.1073/pnas.1411762111>.
- Leidwanger, J., 2019. The Knidia and its amphoras: taking stock of a regional agricultural economy. *HEROM: Journal on Hellenistic and Roman Material Culture* 8, 237–255. <https://doi.org/10.1400/276582>.
- Leidwanger, J., 2020. *Roman Seas: A Maritime Archaeology of Eastern Mediterranean Economies*. Oxford University Press, New York.
- Leidwanger, J., Greene, E.S., Tuna, N., 2015. A late antique ceramic assemblage at Burgaz, Datça Peninsula, South-west Turkey, and the ‘normality of the mixed cargo’ in the ancient Mediterranean. *Int. J. Naut. Archaeol.* 44, 300–311. <https://doi.org/10.1111/1095-9270.12110>.
- Lespez, L., Lescure, S., Saulnier-Copard, S., Glais, A., Berger, J.-F., Lavigne, F., Pearson, C., Virmoux, C., Müller Celka, S., Pomadère, M., 2021. Discovery of a tsunami deposit from the Bronze Age Santorini eruption at Malia (Crete): impact, chronology, extension. *Sci. Rep.* 11, 15487. <https://doi.org/10.1038/s41598-021-94859-1>.
- Lisé-Pronost, A., Salomon, F., Goiran, J.-P., St-Onge, G., Herries, A.I.R., Montero-Serrano, J.-C., Heslop, D., Roberts, A.P., Levchenko, V., Zawadzki, A., Heijns, H., 2019. Dredging and canal gate technologies in Portus, the ancient harbour of Rome, reconstructed from event stratigraphy and multi-proxy sediment analysis. *Quat. Int.* 511, 78–93. <https://doi.org/10.1016/j.quaint.2018.05.018>.
- Longman, J., Veres, D., Ersek, V., Tamas, C.G., Haliuc, A., Magyari, E., Gogaltan, F., Panajotidis, S., Papadopoulou, M., 2024. Central-Eastern Europe as a centre of Middle Ages extractive metallurgy. *J. Archaeol. Sci.* 172, 106093. <https://doi.org/10.1016/j.jas.2024.106093>.
- Marriner, N., Morhange, C., 2006. Geoarchaeological evidence for dredging in Tyre’s ancient harbour, Levant. *Quat. Res.* 65, 164–171. <https://doi.org/10.1016/j.yqres.2005.07.004>.
- Marriner, N., Morhange, C., 2007. Geoscience of ancient Mediterranean harbours. *Earth Sci. Rev.* 80, 137–194.
- Marriner, N., Morhange, C., Doumet-Serhal, C., 2006. Geoarchaeology of Sidon’s ancient harbours, Phoenicia. *J. Archaeol. Sci.* 33, 1514–1535. <https://doi.org/10.1016/j.jas.2006.02.004>.
- Marriner, N., Flaux, C., Morhange, C., Kaniewski, D., 2012. Nile Delta’s sinking past: quantifiable links with Holocene compaction and climate-driven changes in sediment supply? *Geology* 40, 1083–1086. <https://doi.org/10.1130/G33209.1>.
- Marriner, N., Kaniewski, D., Morhange, C., Flaux, C., Giaime, M., Vacchi, M., Goff, J., 2017. Tsunamis in the geological record: making waves with a cautionary tale from the Mediterranean. *Sci. Adv.* 3, 12. <https://doi.org/10.1126/sciadv.1700485>.
- Martín-Puertas, C., Valero-Garcés, B.L., Mata, M.P., Moreno, A., Giralt, S., Martínez-Ruiz, F., Jiménez-Espejo, F., 2011. Geochemical processes in a Mediterranean Lake: a high-resolution study of the last 4,000 years in Zöñar Lake, southern Spain. *J. Paleolimnol.* 46, 405–421. <https://doi.org/10.1007/s10933-009-9373-0>.
- Martínez Cortizas, A., López-Merino, L., Silva-Sánchez, N., Sjöström, J.K., Kylander, M.E., 2021. Investigating the Mineral Composition of Peat by Combining FTIR-ATR and Multivariate Analysis. *Minerals* 11, 1084. <https://doi.org/10.3390/min11101084>.
- Mayoral, A., Ejarque, A., García-Molsosa, A., Georgiadis, M., Apostolou, G., Gaertner, V., Kallintzi, C., Kefalidou, E., Orengo, H., 2024. A city against the current: a reconstruction of Holocene sea-level changes and the evolution of coastal landscapes in ancient Abdera (Thrace, Gr.). *Catena* 235, 107638. <https://doi.org/10.1016/j.catena.2023.107638>.
- Milot, J., Blichert-Toft, J., Sanz, M.A., Fetter, N., Telouk, P., Albarède, F., 2021. The significance of galena Pb model ages and the formation of large Pb-Zn sedimentary deposits. *Chem. Geol.* 583, 120444. <https://doi.org/10.1016/j.chemgeo.2021.120444>.
- Morrison, J.S., Coates, J.F., 1986. *The Athenian Trireme: the History and Reconstruction of an Ancient Greek Warship*. Cambridge University Press, Cambridge.
- Morrison, J.S., Coates, J.F., 1996. *Greek and Roman Oared Warships*. Oxbow Books, Oxford.
- Nelson, A.R., Shennan, I., Long, A.J., 1996. Identifying coseismic subsidence in tidal-wetland stratigraphic sequences at the Cascadia subduction zone of western North America. *J. Geophys. Res. Solid Earth* 101, 6115–6135. <https://doi.org/10.1029/95JB01051>.
- Newton, C.T., 1865. *Travels & Discoveries in the Levant*, II. Day & Son, London.
- Nigdelis, P., 2007. The age of the Macedonian kingdom (316–168 B.C.). In: Koliopoulos, I. (Ed.), *The History of Macedonia*. Museum of the Macedonian Struggle Foundation, Thessaloniki, pp. 51–87.
- Ortiz, J.E., Torres, T., López-Cilla, I., Galán, L.A., Sánchez-Palencia, Y., Ros, M., Manteca, I., Ramallo, S., Navarro, F., Rodríguez-Estrella, T., Blázquez, A., Borrego, A.G., Ruiz-Zapata, B., Gil-García, M.J., Heine, E., 2021. Keys to discern the Phoenician, Punic and Roman mining in a typical coastal environment through the multivariate study of trace element distribution. *Sci. Total Environ.* 790, 147986. <https://doi.org/10.1016/j.scitotenv.2021.147986>.
- Özgan, R., 1995. Knidos 1993. *Kazi Sonuçları Toplantısı* 16 (2), 297–314.
- Özsayın, E., Üner, S., Kahraman, B., 2021. Late Quaternary subsidence records from the Datça graben and Cnidus ancient city (SW Turkey): sea-level changes versus tectonics. *Geol. Acta* 19, 1–14. <https://doi.org/10.1344/geologicaActa2021.19.6>.
- Parker, A.J., 1990. Classical antiquity: the maritime dimension. *Antiquity* 64, 335–346. <https://doi.org/10.1017/S0003598X00078005>.
- Patterson, C.C., 1972. Silver stocks and losses in ancient and medieval times. *Econ. Hist. Rev.* 25, 205–233.
- Pernicka, E., Begemann, F., Schmitt-Strecker, S., Wagner, G.A., 1993. Eneolithic and early Bronze Age copper artefacts from the Balkans and their relation to Serbian copper ores. *Praehistorische Z.* 68, 1–54.
- Pirazzoli, P.A., Stiros, S.C., Arnold, M., Laborel, J., Laborel-Deguen, F., Papageorgiou, S., 1994. Episodic uplift deduced from Holocene shorelines in the Perachora Peninsula, Corinth area, Greece. *Tectonophysics* 229, 201–209. [https://doi.org/10.1016/0040-1951\(94\)90029-9](https://doi.org/10.1016/0040-1951(94)90029-9).

- Pleuger, E., Goiran, J.-P., Delile, H., Gadhoum, A., Abichou, A., Wilson, A., Fentress, E., Ben Jerbania, I., Ghozzi, F., Fagel, N., 2019. Exploration of the maritime façade of Utica: the potential location of the Phoenician and Roman harbours. *Quat. Int.* 511, 140–152. <https://doi.org/10.1016/j.quaint.2019.04.007>.
- Reilinger, R., McClusky, S., Paradissis, D., Ergintav, S., Vernant, P., 2010. Geodetic constraints on the tectonic evolution of the Aegean region and strain accumulation along the Hellenic subduction zone. *Tectonophysics, Extensional Tectonics in the Basin and Range, the Aegean, and Western Anatolia* 488, 22–30. <https://doi.org/10.1016/j.tecto.2009.05.027>.
- Reimann, C., 2008. *Statistical Data Analysis Explained: Applied Environmental Statistics with R*. John Wiley & Sons, Chichester. Royaume-Uni de Grande-Bretagne et d'Irlande du Nord.
- Reimer, P.J., Austin, W.E.N., Bard, E., Bayliss, A., Blackwell, P.G., Ramsey, C.B., Butzin, M., Cheng, H., Edwards, R.L., Friedrich, M., Grootes, P.M., Guilderson, T.P., Hajdas, I., Heaton, T.J., Hogg, A.G., Hughen, K.A., Kromer, B., Manning, S.W., Muscheler, R., Palmer, J.G., Pearson, C., Plicht, J., van der, Reimer, R.W., Richards, D.A., Scott, E.M., Southon, J.R., Turney, C.S.M., Wacker, L., Adolphi, F., Büntgen, U., Capone, M., Fahrni, S.M., Fogtmann-Schulz, A., Friedrich, R., Köhler, P., Kudsk, S., Miyake, F., Olsen, J., Reining, F., Sakamoto, M., Sookdeo, A., Talamo, S., 2020. The IntCal20 Northern hemisphere radiocarbon Age calibration curve (0–55 cal kBP). *Radiocarbon* 62, 725–757. <https://doi.org/10.1017/RDC.2020.41>.
- Riddick, N.L., Boyce, J.I., Reinhardt, E.G., Rothaus, R.M., Chomicicki, K.M., McCarthy, F.M.G., 2021. Multi-proxy palaeoenvironmental record of coastal tectonic uplift and abandonment (ca. 6th c. CE) of Lechaion's inner harbour, ancient Corinth, Greece. *Quat. Sci. Rev.* 267, 107080. <https://doi.org/10.1016/j.quascirev.2021.107080>.
- Riddick, N.L., Boyce, J.I., Krezosi, G.M., Şahoglu, V., Erkanal, H., Tuğcu, İ., Alkan, Y., Gabriel, J.J., Reinhardt, E.G., Goodman-Tchernov, B.N., 2022. Palaeoshoreline reconstruction and underwater archaeological potential of Liman Tepe: a long-occupied coastal prehistoric settlement in western Anatolia, Turkey. *Quat. Sci. Rev.* 276, 107293. <https://doi.org/10.1016/j.quascirev.2021.107293>.
- Ruzicka, S., 2012. *Trouble in the West: Egypt and the Persian Empire 525–332 BCE*. Oxford University Press, Oxford.
- Sakarya, I., Atıcı, N., Tuna, N., 2019. Knidian amphorae of the Hellenistic and Late Roman periods at Burgaz (Palaia Knidos). *HEROM: Journal on Hellenistic and Roman Material Culture* 8, 317–339. <https://doi.org/10.1400/276585>.
- Salomon, P., Delile, H., Goiran, J.-P., Bravard, J.-P., Keay, S., 2012. The Canale di Comunicazione Traverso in Portus: the Roman sea harbour under river influence (Tiber delta, Italy). *Géomorphol. Relief, Process. Environ.* 75–90.
- Salomon, F., Goiran, J.-P., Bravard, J.-P., Arnaud, P., Djebbi, H., Kay, S., Keay, S., 2014. A harbour-canal at Portus: a geoarchaeological approach to the Canale Romano: Tiber Delta, Italy. *Water Hist* 6, 31–49. <https://doi.org/10.1007/s12685-014-0099-1>.
- Salomon, F., Keay, S., Carayon, N., Goiran, J.-P., 2016. The development and characteristics of Ancient Harbours—Applying the PADM chart to the case studies of Ostia and Portus. *PLoS One* 11. <https://doi.org/10.1371/journal.pone.0162587>.
- Seeliger, M., Pint, A., Frenzel, P., Feuser, S., Pirson, F., Riedesel, S., Brückner, H., 2017. Foraminifera as markers of Holocene sea-level fluctuations and water depths of ancient harbours — a case study from the Bay of Elaia (W Türkiye). *Palaeogeogr. Palaeoclimatol. Palaeoecol.* 482, 17–29. <https://doi.org/10.1016/j.palaeo.2017.05.017>.
- Şimşek, B., Ergin, M., Evren, M., Türkmen, Ö., Palas, S., Pehlivan, H., Aydemir, B.S., Öcal, F., 2017. Grain size, total heavy mineral and element distribution and control factors of current sediments on the floor of Hisarönü and Datça bays. *Bulletin of the Mineral Research and Exploration*. <https://doi.org/10.19076/mta.83774>, 2017.
- Spratt, T.A.B., 1886. Remarks on the Dorian peninsula and gulf, with notes on a temple of Latona there. *Archaeologia* 49 (2), 345–365.
- Stock, F., Pint, A., Horejs, B., Ladstätter, S., Brückner, H., 2013. In search of the harbours: new evidence of late Roman and Byzantine harbours of Ephesus. In: *Quaternary International, LAC 2012: 2ND International Landscape and Archaeology Conference*, 312, pp. 57–69. <https://doi.org/10.1016/j.quaint.2013.03.002>. Berlin.
- Stock, F., Kerschner, M., Kraft, J.C., Pint, A., Frenzel, P., Brückner, H., 2014. The palaeogeographies of Ephesus (Turkey), its harbours, and the Artemision – a geoarchaeological reconstruction for the timespan 1500 – 300 BC. *Zeitschrift für Geomorphologie, Supplementary Issues* 33–66. <https://doi.org/10.1127/0372-8854/2014/S-00166>.
- Stock, F., Knipping, M., Pint, A., Ladstätter, S., Delile, H., Heiss, A.G., Laermanns, H., Mitchell, P.D., Poyer, R., Steskal, M., Thanheiser, U., Urz, R., Wennrich, V., Brückner, H., 2016. Human impact on Holocene sediment dynamics in the eastern Mediterranean – the example of the Roman harbour of Ephesus. *Earth Surf. Process. Landf.* 41, 980–996. <https://doi.org/10.1002/esp.3914>.
- Stos-Gale, Z.A., Davis, G., 2020. The minting/mining nexus: new understandings of archaic Greek silver coinage from lead isotope analysis. In: *Mines, Metals, and Money: Ancient World Studies in Science, Archaeology and History, Metallurgy in Numismatics*. The Royal Numismatic Society, London, pp. 87–100.
- Stos-Gale, Z.A., Gale, N.H., 2009. Metal provenancing using isotopes and the Oxford archaeological lead isotope database (OXALID). *Archaeol. Anthropol. Sci.* 1, 195–213. <https://doi.org/10.1007/s12520-009-0011-6>.
- Sutherland, R.A., 2000. Bed sediment-associated trace metals in an urban stream, Oahu, Hawaii. *Environ. Geol.* 39, 611–627. <https://doi.org/10.1007/s002540050473>.
- Tomczyk, C., Żabiński, G., 2023. A PCA-AHC approach to provenance studies of non-ferrous metals with combined Pb isotope and chemistry data. *J. Archaeol. Method Theor.* 31, 93–143. <https://doi.org/10.1007/s10816-022-09598-y>.
- Törnqvist, T.E., Wallace, D.J., Storms, J.E.A., Wallinga, J., van Dam, R.L., Blaauw, M., Derkens, M.S., Klerks, C.J.W., Meijneken, C., Snijders, E.M.A., 2008. Mississippi Delta subsidence primarily caused by compaction of Holocene strata. *Nat. Geosci.* 1, 173–176. <https://doi.org/10.1038/ngeo129>.
- Tribouillard, N., Algeo, T.J., Lyons, T., Riboulleau, A., 2006. Trace metals as paleoredox and paleoproduction proxies: an update. *Chem. Geol.* 232, 12–32. <https://doi.org/10.1016/j.chemgeo.2006.02.012>.
- Tuna, N., 1983. Batı Anadolu Kent Devletlerinde Mekan Organizasyonu: Knidos Örneği. Dokuz Eylül University. PhD Dissertation.
- Tuna, N., 1988. Ionia ve Datça Yarımadası Arkeolojik Yüzey Araştırmaları, 1985–1986. Araştırma Sonuçları Toplantısı 5 (1), 303–357.
- Tuna, N., 1995. Datça/Burgaz Kazıları, 1993. Kazı Sonuçları Toplantısı Ankara 16 (2), 283–295.
- Tuna, N., 1997. Burgaz Arkeolojik Kazıları, 1995. Kazı Sonuçları Toplantısı Ankara 18 (2), 255–272.
- Tuna, N., 1998. Burgaz Arkeolojik Kazıları 1996 Yılı Çalışmaları. Kazı Sonuçları Toplantısı Ankara 19 (2), 445–464.
- Tuna, N., 2004. Burgaz Kazısı 2002 Yılı Çalışmaları. Kazı Sonuçları Toplantısı Ankara 25 (2), 61–72.
- Tuna, N., Sakarya, İ., Koparal, E., 2009. The preliminary results of Burgaz excavations within the context of locating Old Knidos. In: Rumscheid, F. (Ed.), *Die Karer und die Anderen. Presented at the Internationales Kolloquium an der Freien Universität Berlin, Bonn*, pp. 517–532.
- Tuna, N., Atıcı, N., Sakarya, İ., Greene, E.S., Leidwanger, J., 2014. Burgaz (Palaia Knidos) 2012 Yılı Çalışmaları. Kazı Sonuçları Toplantısı 35 (1), 60–75.
- Tylecote, R.F., 1992. *A History of Metallurgy*. Institute of Materials, London.
- Vacchi, M., Rovere, A., Chatzipetros, A., Zourou, N., Firpo, M., 2014. An updated database of Holocene relative sea level changes in NE Aegean Sea. *Quaternary International, SEQS 2012 Sardinia: at the Edge of the Sea* 328–329, 301–310. <https://doi.org/10.1016/j.quascirev.2013.08.036>.
- Vacchi, M., Marriner, N., Morhange, C., Spada, G., Fontana, A., Rovere, A., 2016. Multiproxy assessment of Holocene relative sea-level changes in the western Mediterranean: Sea-level variability and improvements in the definition of the isostatic signal. *Earth Sci. Rev.* 155, 172–197. <https://doi.org/10.1016/j.earscirev.2016.02.002>.
- Vandarakis, D., Panagiopoulos, I.P., Loukaidi, V., Hatiris, G.-A., Drakopoulou, P., Kikaki, A., Gad, F.-K., Petrakis, S., Malliouri, D.I., Chatzinaki, M., Morfis, I., Kanellopoulos, T.D., Kapsimalis, V., 2021. Assessment of the coastal vulnerability to the ongoing sea level rise for the exquisite Rhodes island (SE Aegean Sea, Greece). *Water* 13, 2169. <https://doi.org/10.3390/w13162169>.
- Vaxevanopoulos, M., Blichert-Toft, J., Davis, G., Albarède, F., 2022. New findings of ancient Greek silver sources. *J. Archaeol. Sci.* 137, 105474. <https://doi.org/10.1016/j.jas.2021.105474>.
- Véron, A., Goiran, J.-P., Morhange, C., Marriner, N., Empereur, J.Y., 2006. Pollutant lead reveals the Pre-Hellenistic occupation and ancient growth of Alexandria, Egypt. *Geophys. Res. Lett.* 33, 1–4. <https://doi.org/10.1029/2006GL025824>.
- Véron, A.J., Flaux, C., Marriner, N., Poirier, A., Rigaud, S., Morhange, C., Empereur, J.-Y., 2013. A 6000-year geochemical record of human activities from Alexandria (Egypt). *Quat. Sci. Rev.* 81, 138–147. <https://doi.org/10.1016/j.quascirev.2013.09.029>.
- Vött, A., Bruins, H.J., Gawehn, M., Goodman-Tchernov, B.N., De Martini, P.M., Kelletat, D., Mastromuzzi, G., Reicherter, K., Rötbke, B.R., Scheffers, A., Willershäuser, T., Avramidis, P., Bellanova, P., Costa, P.J.M., Finkler, C., Hadler, H., Koster, B., Lario, J., Reinhardt, E., Mathes-Schmidt, M., Ntageretzi, K., Pantosti, D., Papanikolaou, I., Sansò, P., Scicchitano, G., Smedile, A., Szczucinski, W., 2018. Publicity waves based on manipulated geoscientific data suggesting climatic trigger for majority of tsunami findings in the Mediterranean – response to ‘Tsunamis in the geological record: making waves with a cautionary tale from the Mediterranean’ by Marriner et al. *Zeitschrift für Geomorphologie Supplementary Issues* 39. <https://doi.org/10.1127/zfg.suppl/2018/0547>, 2017.
- Westner, K.J., Birch, T., Kemmers, F., Klein, S., Höfer, H.E., Seitz, H.-M., 2020. ROME's rise to power. Geochemical analysis of silver coinage from the western Mediterranean (fourth to second centuries BCE). *Archaeometry* 62, 577–592. <https://doi.org/10.1111/arcm.12547>.
- Westner, K.J., Vaxevanopoulos, M., Blichert-Toft, J., Davis, G., Albarède, F., 2023. Isotope and trace element compositions of silver-bearing ores in the Balkans as possible metal sources in antiquity. *J. Archaeol. Sci.* 155, 105791. <https://doi.org/10.1016/j.jas.2023.105791>.
- Westner, K.J., Blichert-Toft, J., Gentelli, L., Pavloska, E., de Callataÿ, F., Albarède, F., 2024. Tracing metallurgical links and silver provenance in Balkan coinage (5th–1st centuries BCE). *Archaeol. Anthropol. Sci.* 16, 198. <https://doi.org/10.1007/s12520-024-02106-1>.
- Wilker, S., Leidwanger, J., Greene, E.S., 2019. Amphoras and the afterlife of a commercial port: Hellenistic Burgaz on the Datça (Knidos) Peninsula. *HEROM: Journal on Hellenistic and Roman Material Culture* 8, 357–381. <https://doi.org/10.1400/276587>.
- Younes, G., Kaniewski, D., Marriner, N., Morhange, C., Sheisha, H., Odler, M., Wang, Y., Chen, Z., El-Qady, G., Saleem, A., Véron, A., 2024. The construction of the Giza pyramids chronicled by human copper contamination. *Geology*. <https://doi.org/10.1130/G51965.1>.